Design and Analysis of Generic Hypersonic Scramjet Inlets

N. Om Prakash Raj

A Thesis Submitted to
Indian Institute of Technology Hyderabad
In Partial Fulfillment of the Requirements for
The Degree of Master of Technology

भारतीय प्रौद्योगिकी संस्थान हैदराबाद
Indian Institute of Technology Hyderabad

Department of Mechanical Engineering

June 2012

Declaration

I declare that this written submission represents my ideas in my own words, and where ideas or words of others have been included, I have adequately cited and referenced the original sources. I also declare that I have adhered to all principles of academic honesty and integrity and have not misrepresented or fabricated or falsified any idea/data/fact/source in my submission. I understand that any violation of the above will be a cause for disciplinary action by the Institute and can also evoke penal action from the sources that have thus not been properly cited, or from whom proper permission has not been taken when needed.

N. Om Prakash Raj

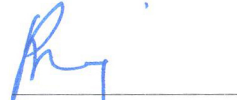(Signature)

_____

(N. Om Prakash Raj)

ME10M05

(Roll No.)

Approval Sheet

This Thesis entitled "Design and Analysis of Generic Hypersonic Scramjet Inlets" by "N. Om Prakash Raj" is approved for the degree of Master of Technology from IIT Hyderabad

(Dr. Vinod Janardhanan) Examiner
Dept. of Chemical Engg.
IITH

(Dr. Raja Banerjee) Examiner
Dept. Mechanical Engg
IITH

(Dr.K. Venkatasubbaiah) Adviser
Dept. Mechanical Engg
IITH

(Dr. Narasimha Mangadoddy) Chairman
Dept. of Chemical Engg.
IITH

Acknowledgements

The work presented here would not have been possible without the guidance and support of many people who in one way or the other extended their valuable assistance. I take this opportunity to express my sincere gratitude towards them.

First and foremost, I would like to thank my advisor Dr.K.Venkatasubbiah for his phenomenal guidance and support. I am deeply grateful for his valuable mentoring and supervision during the course of this thesis work. I have learnt so much in the countless hours of discussions we had in which he has patiently explained all the intricate concepts in a simple manner. Apart from the technical inputs, I'm also thankful for his moral support in my life and career. He has inspired and motivated me to work hard and to always move forward. Working with him has been a wonderful experience for me.

I would like to express my sincere thanks to Prof.Vinayak Eswaran and Dr.Raja Banarjee who have inspired me and taught me many things during my stay at IIT Hyderabad. It has been my privilege to gather knowledge from the brightest minds.

I am greatly in debt to my friends in ThermoFluid family especially Ravi Salgar, Amit Dighe, Raja Jaya Singh and Mrunalini for being there with me at all times. I sincerely acknowledge their encouragement and assistance that I received during the course of our masters program. I can never forget the countless hours spent in lab doing assignments and debugging CFD codes with them. I am sure all of our sleepless nights and restless days spent in IIT Hyderabad will be paid off.

I am very much grateful to Librarian Mallikarjun who has got me papers and text books, without which this work couldn't have been finished. I am also thankful to my lab mates Mr. Madhu, Mr.Srikanth and Ms.Nagalakshmi for being on my side and providing valuable support during my thesis work. I'm very thankful to Nagarjuna who has helped me in developing SIG application. I'm also grateful to my juniors Nitish, Patel, Mudassar, Nikhil, Pankaj and Amit who have helped me to expand my knowledge and for all the warmth I received. I also thank Saritha and Santosh for their valuable inputs.

Finally, I thank my family for all the constant love and support I received throughout the years. The satisfaction of completing this work would have been meaningless without having my family by my side throughout the entire process. I am thankful to God for providing me with all the resources and showing me the right path.

Dedicated to my loving family

Abstract

A new methodology has been developed for the design of hypersonic scramjet inlets using gas dynamic relations. The approach aims to find the optimal inlet geometry which has maximum total pressure recovery at a prescribed design free stream Mach number. The design criteria for inlet is chosen as *shock-on-lip condition* which ensures maximum capture area and minimum intake length. Designed inlet geometries are simulated using CFD analysis. The effects of 1D, 2D, inviscid and viscous effects on performance of scramjet inlet are reported here. A correction factor in inviscid design is reported for viscous effects to obtain *shock-on-lip* condition. A parametric study is carried out for the effect of throat Mach number in the design of scramjet inlets. Present results show that 2D and viscous effects are significant on performance of scramjet inlet. Performance analysis of scramjets inlets has also been performed. Two planar inlets Mach 10.4 and Mach 7 are considered and the effects of wall cooling, off design and cowl height on the performance of the scramjet inlets are reported. Various performance parameters of scramjet inlets are reported with different operating conditions. Maximum temperatures attained in the inlets are given. Results show that the surface temperature and the cowl height have a significant effect on performance of scramjet inlet. The total pressure recovery coefficient and the spillage losses are reported at different free stream Mach numbers. External flow field analysis is carried out and coefficients of drag and lift are reported here. The Present results are matching well with the experimental results available in the literature.

Contents

Nomenclature

β oblique shock angle

θ turning angle / ramp angle

A_c cross sectional area at cowl

A_t cross sectional area at throat

c_d coefficient of drag

c_l coefficient of lift

M_0 free stream Mach number

m_0 mass flow rate at inlet

m_c mass flow rate at cowl

M_e Mach number after external compression

M_t Mach number at throat

M_{exit} Mach number at exit of isolator

P_0 free stream static pressure

P_{exit} static pressure at exit of isolator

P_{t_0} free stream total pressure

$P_{t_{exit}}$ total pressure at exit of isolator

T_0 free stream static temperature

T_w wall temperature

x_i x - coordinate of geometry

x_{cs} x - coordinate of cowl

y_i y - coordinate of geometry

y_{cs} y - coordinate of cowl

L   Reference length

SPR   static pressure recovery coefficient

TPR   total pressure recovery coefficient

Chapter 1

Introduction

One of the current interests in aerospace research is to develop faster and efficient propulsion systems capable of operating at wider range of operating conditions. With the advent of modern Gas turbine engines and Rockets, aviation technology has transformed from low speed subsonic aircrafts to high payload capacity supersonic aircrafts. With Rockets and turbo engines approaching their limits of operation, a need for efficient engines capable of operating at supersonic and hypersonic regimes is on the rise. In this regard, there has been a great need to make engines more efficient and lighter in weight in order to increase the overall payload capabilities of the vehicle. Thus the dawn of air breathing engines began in the year 1913 when Rene Lorin[1] first granted a patent for the concept of ramjet and eventually led to the development of Supersonic combustion ramjet i.e. scramjet.

The important differences between rockets and airbreathing engines as described by Antonio Ferri[2] are:

1.Specific impulse of airbreathing propulsion is larger than rocket because it carries only fuel but not oxidizer.
2.Thrust of an airbreathing engine is a function of flight Mach number and altitude.
3.Airbreathing vehicle has greater maneuverability than rocket propelled vehicle

After nearly half a decade of research, the first ramjet powered aircraft named Leduc 0.10 was developed by the works of Ren Leduc in 1945. Soon after, developments began in field of ramjet engines and were soon extended to greater domains. One of the notable supersonic aircraft is SR-71 Blackbird, an advanced long-range, a Mach 3 strategic reconnaissance aircraft deployed in late 1960s employing ramjet engine for flight. Since 1976, it has held the world record for the fastest air-breathing manned aircraft and became a marvel in the field of air-breathing engine powered aircrafts. Ramjet technology has also proved to be a great asset in supersonic missiles and one highly distinguishable example is the development of BrahMos. It is a stealth supersonic missile which can be launched

from almost anywhere from submarines, ships, land and air . This has been developed by a joint venture between India and Russia; it is the world's fastest cruise missile in operation. Deployed by Indian Army in 2006, it has reached speeds of Mach 2.83 and there are plans to develop hypersonic missiles which can operate above Mach 7 by the year 2016.

Another advancement in the field of air-breathing engines is scramjet engine. A scramjet engine operates at high velocity regime normally at hypersonic speeds above Mach 5. Although there are cases where it can be operated below Mach 5, instead ramjets are best suited for this. It is an extension of ramjet engine and the basic difference between them lies in the speeds at which combustion takes place. Rockets carry oxygen and they are totally independent of what environment they're operating on. Scramjet doesn't require carrying oxygen as it burns its fuel using surrounding atmospheric air. This increases the overall propulsion systems efficiency of the vehicle as the weight of the aircraft is reduced. But the main drawback of scramjet engines is that they cannot provide thrust at speeds below Mach 3. Therefore it requires an external means to accelerate to speeds where in scramjets provide thrust. For this purpose an integrated Rocket- scramjet propulsion systems are employed, where in the rocket provides the initial thrust and then scramjet takes over.

1.1 History

There has been a tremendous research on high speed propulsion systems pre and post World War II. When Bell X-1 attained supersonic flight in 1947, progress towards developing supersonic and hypersonic aircraft has begun. Early research on supersonic combustion ramjet (scramjet) engines and started in the mid 1950s. The intent was to demonstrate that both thrust and lift can be produced bottom side of the wings when the vehicle is flying at supersonic or hypersonic speeds. During 1950s and 1960s a wide variety of experimental scramjet engines are tested in US and UK.

In 1958 at NASA centers, the phenomenon of generating thrust has been demonstrated by an experiment involving a double wedge at Mach 5 stream. Supersonic combustion has been demonstrated in this experiment and this project has continued until 1961. The work of Antonio Ferri at the beginning of the 1960s made a substantial contribution to the understanding of mixing and diffusive combustion processes in supersonic flows and was, to a large extent, the major driver for the technological developments that are carried out later.

Large research projects such as the NASAs Hypersonic Research Engine (NASA-HRE) project have started in 1960s. Their ultimate goal was to build and test a hypersonic research ramjetscramjet engine in flight using X- 15A-2 research airplane that has been
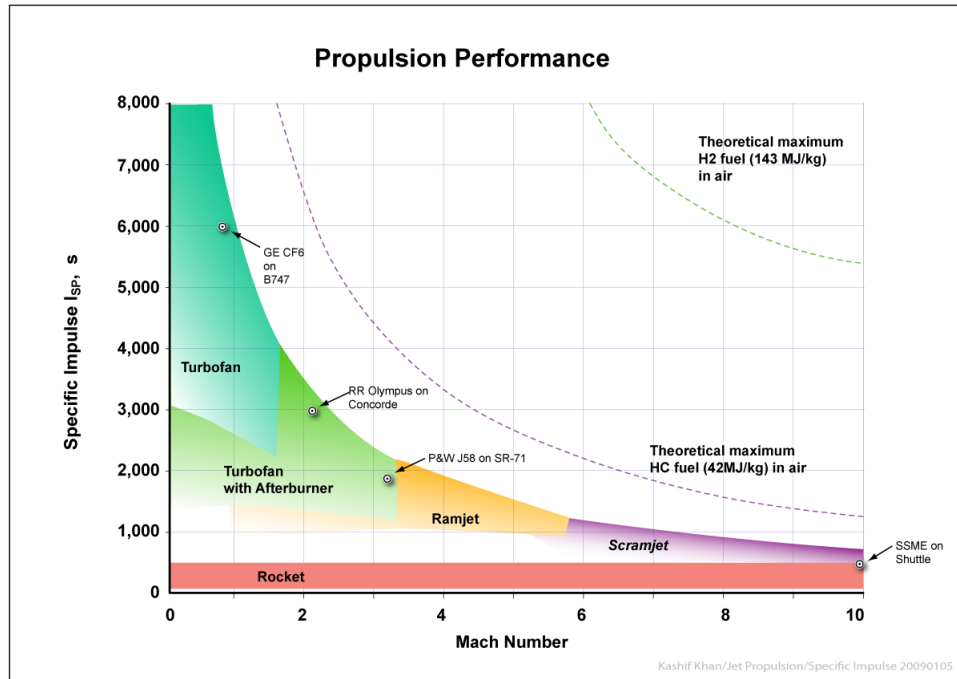
Figure 1.1: Specific impulse of various engines

modified to carry hydrogen as the fuel for the scramjet engine. Meanwhile in USSR, with the work of Shchetinkov in late 1950s researchers have focused on the issues such as chemical conversion efficiency at higher temperatures, heat transfer at low pressure conditions and design operations efficiency. Contributions from this research has extended to combined cycle engines for scramjet operation and liquid-air collection engines by Andrews and Mackley[3].

National Aerospace Plane (NASP) program in the united states has started to create a single-stage-to-orbit spacecraft and passenger space liner (see Fig.1.2). A lot of developmental work has been carried out in advanced materials, propulsion, sustainability and flight control. Most significant achievement of the research undertaken in this project was the development of predictive tools in the area of computational fluid dynamics, with applications to both external aerodynamics and internal flows with chemical-reaction modeling for propulsion applications. The project was canceled in the early 1990s before a prototype was completed.

In 1964, Frederick S. Billig and Gordon L. Dugger submitted a patent application for a supersonic combustion ramjet based on Billigs Ph.D. thesis [4]. Later in 1981, ground based scramjet tests have been done in Australia under the guidance of Prof Ray Stalker in the T3 ground test facility at Australian National University. In the year 1991, first successful scramjet flight was carried out by Russia. It is an axi-symmetric hydrogen-fueled

Figure 1.2: Artist's Concept of the X-30 of NASP program

dual-mode scramjet developed by Central Institute of Aviation Motors (CIAM). Additional flight tests that are conducted by CIAM together with France and then with NASA, USA.

Different U.S Organizations accepted hypersonic flight as a common goal and Defense Research Development Organization of India with its program, Hypersonic Technology Demonstrator Vehicle (HSTDV) is expected to develop an unmanned scramjet aircraft. NASA's Hyper-X program has been tailored to move hypersonic airbreathing technology from laboratory environment to the flight environment. Through this program X-43 an unmanned experimental hypersonic aircraft is developed and recently a third version of it flew in 2004 attaining 34Km altitude and a speed record of Mach 9.8. Boeing X-51 Waverider an unmanned scramjet demonstration vehicle has completed its first free flight on May 2010 at speeds over Mach 5 and set a record for longest scramjet burn time of 140 seconds preceding X-43 time of 12 seconds.

1.2 Fundamental description

A hypersonic air-breathing engine uses surrounding air as oxidizer for combustion of fuel and performs this operation without any moving components. It is this characteristic which separates ramjet and scramjet engines from gas turbine and rocket engines. Basic operation of ramjet and scramjet engine is same except that in ramjet combustion takes place in subsonic velocities where as in scramjets it is supersonic throughout.
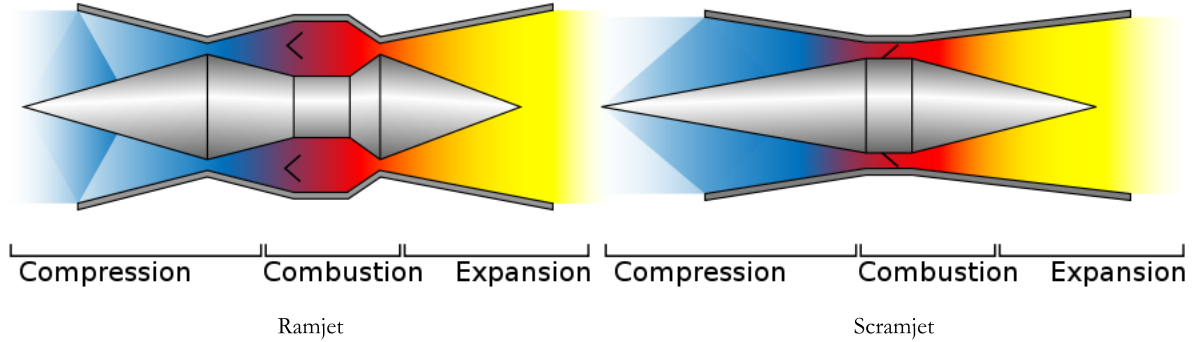

Figure 1.3: Schematic of ramjet and scramjet engines

Schematically, difference between ramjet and scramjet geometries is shown in Fig.1.3. It is evident that the only difference between them is the existence of a physical throat in nozzle section of ramjet engine. For subsonic conditions to prevail in the combustion chamber, presence of a physical throat is required. In supersonic combustion chamber i.e. for scramjets, an area increase is required to release the heat through combustion. A series of oblique shocks exists in the inlet section which compresses the incoming air and delivers to the diffuser section to further process the flow. Inside the scramjet engine the flow is supersonic throughout and Mach is always greater 1. In simple terms, inlet compresses the air, isolator delivers the air to the combustion chamber at supersonic velocities, and fuel is mixed with the incoming air and is burnt in combustion chamber. Finally gas is expanded and accelerated at supersonic velocities in the nozzle providing thrust. The kinetic energy of the free stream air is large compared to the total energy released by the reaction of fuel and oxidizer. Higher velocities result in even smaller fractions of the total enthalpy of the working fluid coming from fuel combustion. Hence it is a major concern in scramjet design to make sure that as large a fraction as possible of the supplied fuel really reacts.

The design of a scramjet engine depends on two factors. Firstly, the temperature of the compressed air flowing into the combustor must be high enough for combustion to take place, and secondly, there must be enough pressure for the complete reaction to occur before the gases are hurtled out through the back of the engine. These requirements on the incoming air are the main reason for the characteristic funnel-like design of the air inlet.

The air flowing into the inlet is compressed by the forward velocity of the vehicle through the atmosphere. This means that a scramjet, just like a ramjet, requires a certain speed before it can be started at all. The minimum operating Mach number at which a scramjet can operate is therefore limited by the pressure of the incoming airflow as well as the temperature. Moreover, for the engine to be called a scramjet the compressed flow must be supersonic even after combustion.

Compression of a supersonic flow firstly leads to the deceleration of the flow. This implies that the free stream air speed must be high enough for the air flow not to be slowed down below Mach 1. If the flow in a scramjet engine goes below Mach 1 the engine is said to choke, transitioning to subsonic flow in the combustion chamber. Secondly, the heating of a gas causes the local speed of sound in the gas to increase, in which the Mach number decreases, despite the fact that the gas flows with the same velocity as before the heating. There is no distinct lower limit for scramjet operation, but a fair estimation is that the engine will need a speed of at least Mach 4-5 to be able to maintain fully supersonic combustion.

1.3   Scramjet component analysis

Fig.1.4 shows a schematic of the internal flowpath of a scramjet vehicle with reference stations highlighted. Station 0 is in the freestream flow ahead of the engine, and a stream tube with area A_0 is captured and processed by the engine. Station 1 is downstream of the vehicle forebody and represents the properties of the flow that enters the inlet. Station 2 is at the inlet throat, which is usually the minimum area of the flowpath, and the length between stations 2 and 3 is referred to as the isolator. Station 3 represents the start of the combustor, and fuel and air is mixed and burned by the end of the combustor at station 4. The nozzle includes an internal expansion up to station 9, and an external expansion to station 10 at the end of the vehicle as reported in [5].
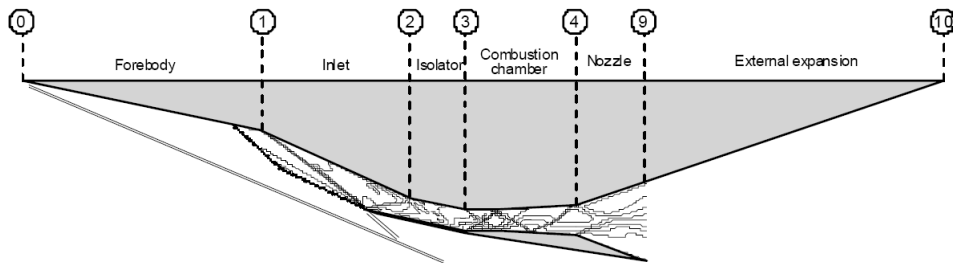

Figure 1.4: Flow stations of scramjet vehicle

1.3.1   Compression

For efficient combustion to take place, it is required that the air is supplied to the combustor at a suitable pressure, temperature and flow rate. For a scramjet, which operates at very high velocities and altitude, it is necessary to have significant compression and heating of the air before being processed into the combustion chamber. For an airframe integrated scramjet, both the vehicle forebody and the inlet share this task. Different forebody/inlet configurations have been developed by many researchers, each designed to generate a specified level of compression over a range of flight Mach numbers.

The performance of a compression system can be specified by two parameters:

1. Amount of compression achieved

2. Total pressures losses

In order to determine the inlet efficiency, both these parameters have to be considered. Efficiency of an inlet greatly depends on the geometrical configuration of the inlet. It is therefore important for a designer that in order to have minimum pressure losses, the inlet geometry have to be designed in a way so as to achieve this. Inlet consists of series of oblique shocks which compress the air as it passes through and at the same time turns the flow towards the combustion chamber. The main goal is to control these oblique shocks so as to improve the inlet efficiency. The process of establishing supersonic flow through the inlet puts a significant constraint on the internal contraction ratio of hypersonic inlets. This can be overcome through variable geometry; however, the weight/complexity of such can significantly degrade the overall system performance of a scramjet engine. Theoretical starting limit known as Kantrowitz limit puts a limit on the contraction ratio at different Mach numbers.

The flow through any practical hypersonic inlet will be turbulent, and can be prone to boundary layer separation due to shock interactions. While minor boundary layer separation may be acceptable, large-scale boundary layer separation can create blockage of the engine and inlet unstart. Inlet is therefore required to satisfy established boundary layer separation limits.

The minimization of external drag is an important aspect of the inlet design process. The external drag on the inlet will always be an important parameter when comparing the performance of different inlet configurations. Finally, most inlet design methods are based on a particular design Mach number, usually at the upper limit of the operational Mach number range. Adequate off-design performance; i.e. at Mach numbers lower than the design point, is required, otherwise the vehicle will never reach its design point.

1.3.2 Combustion

Combustion in a scramjet engine can generate large pressure rise and separation of boundary layer on the surface of the combustion chamber. This separation, if it propagates into the inlet chamber can effect the compression process and may even unstart the engine. In order to avoid this, a short duct called as isolator is kept between the inlet and the combustion chamber to contain this phenomenon. Essentially, the purpose of the isolator is stop the effects of the combustion from propagating upstream into the inlet.

In the design of scramjet combustors there are some key issues that must be addressed in order to arrive at a useful configuration. These are:
1. Adequate mixing of fuel and air
2. Fuel ignition and flame holding
3. Operation over a range of inflow conditions

1.3.3 Expansion

The expansion process converts the potential energy of the combusting flow to kinetic energy and then thrust. In a scramjet, this begins in the divergent sections of the combustor and internal nozzle, and continues over a large portion of the vehicle afterbody. Afterbody shape also determines the direction of net thrust of the scramjet vehicle.

The design of nozzle expansion systems for airframe-integrated scramjet vehicles is one of the least mature aspects of overall design process. This may be due to the historical separation of the propulsion and airframe, with neither groups wanting to take full responsibility for the engine nozzle/vehicle afterbody. But the confidence that these issues can be solved for practical vehicles was significantly increased by the successful flights of the NASAs Hyper-X vehicle.

1.4 Literature survey

Scramjet propulsion system design has been interest of study since past few years and scramjets are preferred when compared to rocket propulsion system because of its light weight, high specific impulse and greater potential for maneuverability as given in Curran and Murthy [6]. There are three types of scramjet inlets; (i) External compression inlet, (ii) Internal compression inlet and (iii) Mixed compression inlet. Among which, mixed compression inlet has the advantage of having low drag, shorter intake length and high pressure ratio potential as reported in Heiser and Pratt [7]. Mixed compression inlet can be designed by the following two approaches: one aiming at maximizing total pressure recovery and another aims of design at prescribed Mach number at the throat. By employing these two approaches independently, supersonic inlet was designed and the effects of on-design and off-design conditions on performance of inlet at different flight Mach numbers were reported in Valorani *et.al.*[8].

One of the first attempts in developing an optimal design for supersonic inlet which reduces to subsonic flow was done by Oswatitsch[9]. By using gas dynamic relations and Lagrange multipliers and with an objective of maximum total pressure recovery, a set of oblique shock angles and one terminating normal shock angle were obtained. It has been observed that in order to improve the compression efficiency, shocks have to be of equal strength (Oswatitsch criterion). Extension of this analogy for scramjet inlet was done by Smart [10], where the inlet was optimized based on maximum total pressure recovery and Oswatitsch criterion is also observed. It is also found that total pressure recovery increases with an increase in number of shocks.

Efficient functioning of a supersonic vehicle is determined by integration of various systems, among which inlet plays a vital role in optimum compression. Description of flow fields in supersonic combustion at fundamental aspects has been given in Billig [11].Design requirements of isolator being the system which connects inlet and combustion chamber were reported by Billing and Kothari [12]. Various experimental and computational investigations were performed to know the effect of isolator lengths on performance of scramjet inlet by Reinartz and Hermann [13].

Design of supersonic missile inlet using automated optimization with CFD analysis was reported in Smith *et.al.* [14].In another approach Bilevel Integrated System Synthesis (BLISS) method was used for optimization of scramjet inlet and flow phenomena in three subsystems of scramjet: inlet, combustor and nozzle was studied using CFD Xuxu *et.al.*[15]. Optimization was done using one dimensional gas dynamic relations. Avoiding the separation region and improvement of scramjet performance were reported using CFD analysis. Another aspect that has to be considered in design of inlet is to establish supersonic flow

through the inlet without causing inlet to unstart. These issues are reported in Kantrowitz and Donaldson[16] and theoretical starting limit known as Kantrowitz limit which puts a restriction on area. Kantrowitz limit is defined as ratio of areas at the throat to the inlet. By experiments it is observed that scramjet inlet unstarts if Kantrowitz limit is not satisfied as reported in Smart and Trexler[17].

Inlet unstart is also caused by the presence of separation regions which choke the scramjet inlet as reported by Delery[18]. Mach number at throat is also an important parameter for design of inlet because which has significant effect on formation of separation region. The formation of separation regions was observed experimentally by Mahoney[19] if the Mach number at the throat is less than 50% of the free stream Mach number. Inlet starting has been studied and been found to be dependent on Mach number, internal contraction ratio, pressure recovery coefficient and time dependence of starting process by Andrews *et.al.* and Wie *et.al.* [20, 21]. Classification of hypersonic inlet unstart phenomenon based on different operating parameters has been given in Chang *et.al* [22]. Large separation regions causes unstart of inlet and when separation is unavoidable; various techniques such as bleeding or blowing to control the separation has been discussed in Hamed and Shang [23].

The phenomenon of shock-wave/boundary layer interactions on performance of scramjet inlets has been discussed in Stollery [24]. Internal flow field characteristics have been studied experimentally and numerically for scramjet inlet at Mach 10 and found that cowl height is one of the important parameters for operation of scramjet inlet Van Wie and Ault [25]. As very high temperatures are generated inside the vehicle, it is evident that scramjets need cooling and in this regard experimental and numerical investigations have been performed on endothermic fuel cooling for scramjet applications Daniau and Sicard [26]. It has been reported that wall cooling influences various performance parameters of scramjet inlet by weakening shock-wave/boundary layer interactions Chang *et.al* [27].

Research has also been done in the design of 3D hypersonic inlets by Smart[28]. In this study, inviscid stream tracing technique was used for design of inlet with rectangular to elliptical shape transition and is also tested experimentally in Smart[29]. Experimental tests were conducted for mixed compression inlet to study the viscous effects on inlet flow field parameters and found that passive bleeding reduce the separation regions by Haberle and Gulhan[30]. It is found that cowl position is one of the important parameter for operation of scramjet inlet. CFD has evolved up to an extent where complex phenomenon of hypersonic propulsions can be modeled and these CFD simulations have become important means to study the physics of scramjet engines and these are discussed by Povinelli and Drummond *et.al.* [31, 32].A full flow path analysis of a hypersonic vehicle at Mach 7 is carried out computationally by Shu *et.al.*[33] and the aerodynamic characteristics of the

vehicle are studied. It is found that inlet started and unstarted operations has significant effect on the flow pattern of the inlet.

Charles and Lawrence[34] have performed computational analysis for a single hypersonic inlet module to obtain the internal drag force on the inlet region. They carried out 2D and 3D inviscid and viscous CFD analysis of inlet flow field and obtained internal drag force predictions which were compared with the drag obtained from experimental pressure data. Hypersonic flow is studied numerically by Benson *et.al.*[35]and it is found that inlet at Mach 11.3 would experience strong shock/boundary layer interactions and would experience large flow separations and might lead to inlet unstart. A combined experimental and computational study is carried out by Holland [36]for a Mach 10 scramjet inlet to study the nature and structure of internal flow interactions and to determine the effects of contraction ratio and Reynolds number on the performance of hypersonic scramjet inlet.

1.5 Motivation

Currently in the literature a design procedure doesn't exist which aims to find the optimal geometry of scramjet engine inlet at a prescribed throat Mach number. Research only exists in developing a scramjet inlet which aims at improving the overall total pressure recovery or to design an inlet at a prescribed Mach number at throat. A design approach which combines these two methodologies is required.When this approach is made, then the scramjet designer can easily design different inlet configurations at the same time having maximum total pressure recovery. Also in the literature (i) Detailed numerical study does not exist for scramjet inlet flow field and spillage losses with different operating conditions. (ii) Results do not exist to predict maximum temperature attained in the scramjet inlet (iii) Very few studies exist involving the external flow field analysis and the effects of various operating parameters such as cowl height, wall cooling and off-design conditions. These problems have to be addressed in order to address the practical difficulties in operating a scramjet in realtime flight conditions. These have motivated the current research and an objective to find a new approach to design of scramjet inlets and to study the flowfield parameters is realized.

1.6 Objective of current study

Objective of the current study is to present a new approach which aims at design of optimal scramjet inlet at prescribed flight Mach number. The idea is to combine the previous methodologies of inlet design and to develop a design procedure which can generate a scramjet inlet for any number of prescribed external or internal shock combinations. Another goal

is to carry out the internal and external flow field analysis of the scramjet vehicle and to estimate the pressure distributions and wall temperatures and to carry out the performance studies of the scramjet vehicle. The problem statement(s) of the current study is summarized as follows:

- To develop a design methodology which can be used to generate scramjet inlet geometries at any prescribed Mach number.

- To study flow field involving complex shock-shock and shock/boundary layer interactions inside a scramjet inlet.

- To study the inviscid and viscous effects on a scramjet inlet and to obtain a correction equation which finds Mach number at which *shock-on-lip* condition is satisfied in a viscous environment.

- To study the effect of various parameters such as throat Mach number, wall cooling, off-design condition and cowl height on the performance of scramjet inlet

- To study the external flow field of the scramjet vehicle and to estimate the drag and lift coefficients.

Softwares used

- MATLAB 2010b and NetBeans IDE 7.1.1 packages are used for programming.

- Geometry and Meshing is done by using ANSYS ICEM CFD 13.0.

- Computational Fluid Dynamics simulations are done by using ANSYS FLUENT 13.0.

- Postprocessing of the results are carried out by using TECPLOT 360.

Simulations have been carried out alternatively in both Linux and Windows workstations of CPU Quad core x 2.4 GHz, Memory 6GB and CPU Octa core x 2.4 GHz, Memory 8GB respectively.

1.7 Outline of thesis

Chapter. 2 describes a new approach used to design scramjet inlets and a parametric study is carried out to find the effects of Mach number at inlet, after external compression and at throat on total pressure recovery. Kantrowitz limit and the effects of shock combinations on turning angles is also studied. Chapter. 3 deals with numerical analysis of scramjet inlets. A validation study is carried out and the inlets generated by the design procedure were analyzed using CFD and the inviscid and viscous effects are tested. Performance analysis was also carried out for the scramjet inlet and correction for the design to include viscous

effects is also presented. In Chapter. 4, parametric study of various parameters such as throat Mach number, wall cooling, off-design conditions and the effects of cowl heights are presented and their effects on performance of scramjet inlets is presented. Chapter. 5 deals with external flowfield analysis of scramjet vehicle where in surface pressures and surface temperatures are estimated along the scramjet vehicle and the coefficients of lift and drag are reported. Conclusion of the current study is given in Chapter. 6 and scope of future work has been reported in Chapter. 7.

Chapter 2

Inlet Design

2.1 Types of scramjet inlets

Based on type of compression, scramjet inlets fall into three different categories. These are:
1. External compression inlet
2. Internal compression inlet
3. Mixed compression inlet

External inlet configuration is shown in Fig.2.1, as the name implies the compression process takes place externally by series of shock waves along the forebody of the scramjet inlet. Due to the large angle relative to the free stream flow, external compression inlet has large cowl drag. The advantage of external compression inlets is that they are self starting i.e. inlets start without any use of variable geometry and another feature is that these inlets have the ability to spill flow when operating at below design point conditions; this is a desirable feature when operating over a large Mach number range. The schematic of internal compression inlet is shown in Fig.2.2, the whole compression process is done by internal shocks and it mostly is a symmetric along the central plane. Compared to other inlet configurations, this type of inlet has less drag and the length of inlet is smaller than that of external compression inlet. But the disadvantage is that inlet operation at off design conditions may lead to complex flow patterns and extensive variable geometry is required for the inlet to start. Mixed compression inlets (Fig.2.3) perform compression by means of both external and internal shocks. These inlets are typically longer than external compression inlets and also spill flow when operated below design point conditions. Depending on internal compression, mixed compression inlets sometimes require variable geometry for the inlet to start. Having the combined advantages of both external and internal compression inlets, mixed compression is usually preferred and hence in current study mixed compression inlet is chosen.
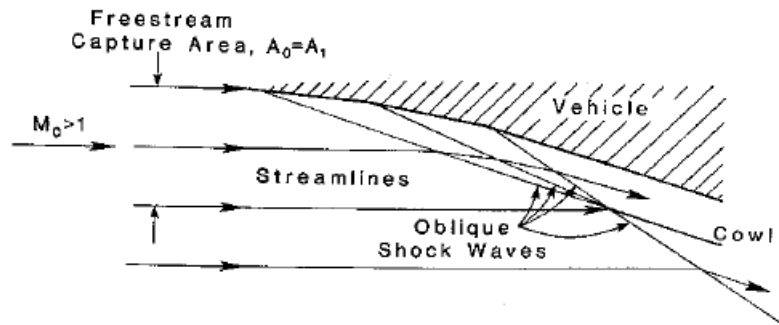
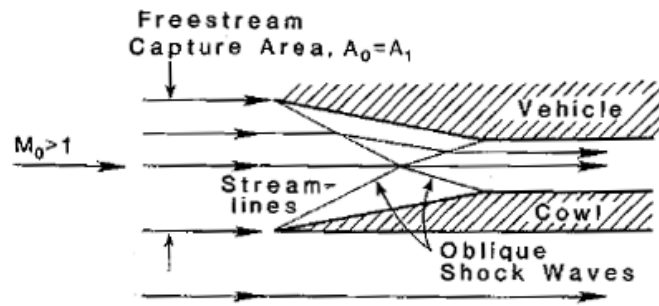Figure 2.1: Schematic of external compression inlet

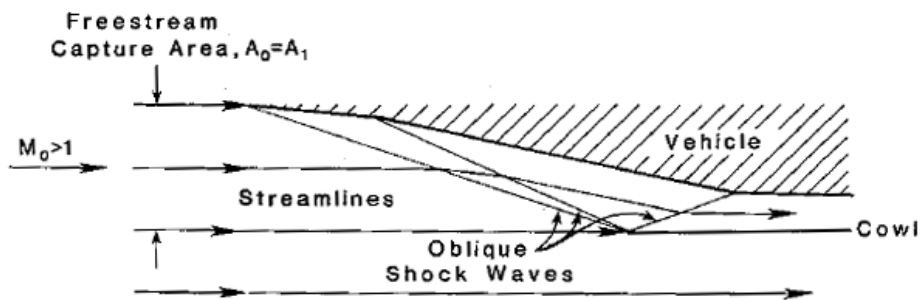Figure 2.2: Schematic of internal compression inlet

Figure 2.3: Schematic of mixed compression inlet
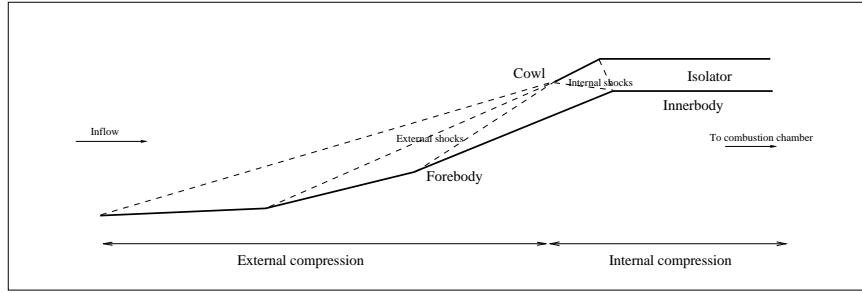
2.2 Design methodology

Figure 2.4: Schematic of mixed compression scramjet inlet depicting various components

As discussed in previous section, mixed compression inlet has the combined advantages of both external and internal compression inlets. Hence for the current study, the objective is to obtain a design procedure for a mixed compression scramjet inlet. The schematic of mixed compression scramjet inlet is shown in Fig.2.4 and various components of the inlet have been mentioned. In this type of inlet, the compression process takes place in two stages (i) External compression and (ii) Internal compression.

The inlet is divided into three sections namely forebody, cowl and innerbody. External compression takes place by means of shocks originating from forebody and internal compression takes place by means of the shocks originating from the cowl. Further compression takes place by means of shock reflections on the innerbody which starts at the end of the forebody and extends until the start of the combustion chamber. The horizontal channel between the cowl and the forebody is termed as isolator. The main purpose of isolator is to isolate the inlet from the effects of the combustion chamber and to contain the backpressures from the combustion chamber from entering into the inlet.

Initially, fluid at a free stream Mach number M_0 passes through series of external shocks which originate along the forebody. In this process the fluid gets decelerated and this reduction in kinetic energy is converted into the pressure energy and thereby compressing the fluid. This compressed fluid again passes between the cowl and the innerbody through a series of internal shocks and enters into the isolator. From the isolator, the compressed flow is delivered into the combustion chamber at supersonic velocities.

Performance of the inlet depends on the number of internal and external shocks and these have to be fixed for the design of inlet. The performance of the scramjet inlet improves with the increase in number of shocks, however isentropic condition puts a limit on number of shocks as given in Valorani et.al. [8]. Moreover, increase in the number of shocks implies decrease in ramp angles and thereby increasing the length of the inlet which adds to overall

weight of the scramjet. Inlet design is divided into two sub stages, to find (i) turning and shock angles and (ii) inlet geometry.

2.2.1   Turning (θ) and Shock (β) angles

The number of external/internal shocks determine the number of turning/ramp angles required. By Oswatitsch criterion [9], in order to increase the efficiency of the inlet, pressure jump across a single shock has to be equally distributed across multiple shocks of equal strength. In order to maximize the inlet compression efficiency, a combination of turning and shock angles are obtained by following an iterative procedure using gas dynamic relations. The free stream Mach number of the scramjet inlet is M_0 and the Mach number at throat i.e. the Mach number after the internal compression is chosen as one half of the free stream Mach number to avoid the flow separation as given by Mahoney[19]. The Mach number after external compression is chosen as the limiting Mach number after the flow turns sonic i.e. when the formation of normal shock is unavoidable.

External compression and the internal compression are divided into two subsystems and the correspond flow turning angles for both external and internal compression are obtained independently. Both the subsystems are independent in design except that the static pressure ratio after the external compression is carried out to the internal compression. This couples the two subsystems. The total pressure across a shock would be maximum, when the static pressure is low and this indicates that weaker shocks are formed. This would occur at low turning angles. Hence, the initial guess values are chosen as static pressure ratio SPR=0.01 and TPR=1.0 and the corresponding shock angle, turning angle, Mach number and total pressure ratio across the shock are obtained at the specified free stream Mach number using the following gas dynamic relations.

$$\beta = \sin^{-1}\left[\sqrt{\frac{\left((SPR - 1)\left(\frac{\gamma+1}{2\gamma}\right)\right) + 1}{M_0^2}}\right] \qquad (2.1)$$

$$\theta = \tan^{-1}\left[2\cot\beta\left(\frac{M_0^2\sin^2(\beta) - 1}{M_0^2\left(\gamma + \cos 2\beta + 2\right)}\right)\right] \qquad (2.2)$$

$$M_1 = \frac{\sqrt{\frac{\left(M_0^2\sin^2(\beta) + \frac{2}{\gamma-1}\right)}{\left(\frac{2\gamma}{\gamma-1}M_0^2\sin^2(\beta) - 1\right)}}}{\sin(\beta - \theta)} \qquad (2.3)$$

$$TPR = \left[\left(1 + \frac{\gamma - 1}{2}M_1^2\right)^{\frac{\gamma}{\gamma-1}}\left(1 + \frac{2\gamma}{\gamma + 1}\left(M_0^2\sin^2(\beta) - 1\right)\right)\left(1 + \frac{\gamma - 1}{2}M_0^2\right)^{\frac{-\gamma}{\gamma+1}}\right] \qquad (2.4)$$

Static pressure ratio of the previous shock is fixed as specified by the Oswatitsch criterion for the next shock and the properties behind the shock are obtained by using the above gas dynamic relations. The same procedure is repeated for all the external shocks. After calculating the values for all the external shocks, the Mach number behind the external shock is compared with the specified Mach number after the external compression i.e. M_e. When both are not equal, then the above procedure is repeated by increasing the static pressure ratio little and iterating until the required value of M_e is reached. When the specified M_e is obtained, then the turning angles for the external compression are obtained.

To obtain turning angles for the internal compression, similar procedure has been followed except that the initial guess is chosen as the static pressure ratio obtained after external compression. The properties behind the internal shocks are obtained by using the same gas dynamic relations and this iteration process is continued by increasing the static pressure ratio a little, until the Mach number after the internal compression is equal to half of the free stream Mach number. Final total pressure ratio of the inlet is obtained by multiplying the total pressure across all the shocks. Optimum turning angles are obtained for maximizing the TPR at prescribed flight Mach number.

2.2.2 Inlet geometry

Turning angles and shock angles for the inlet are obtained by above methodology, but the lengths of the ramps which determine the position of the shocks are also required to complete the design of the scramjet inlet. The schematic of the scramjet inlet showing turning

and oblique shock angles along with the *shock-on-lip* condition is shown in the Fig.2.5. From the Figure. 2.5, a_1a_2 and a_2a_3 are the external ramp angles and a_4a_5 is the internal ramp angle. For convenience, here only two external and one internal shock is mentioned. But there can be any number of external/internal shock combinations limited by the isentropic limit.
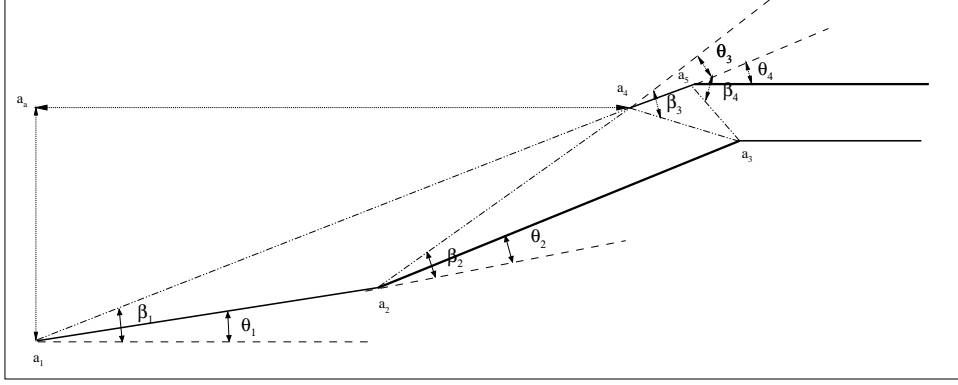

Figure 2.5: Geometrical parameters of scramjet inlet.

Turning angles for a_1a_2, a_2a_3, and a_4a_5 are given by θ_1, θ_2, θ_3 and shock angles β_1, β_2, β_3 respectively which are obtained using gas dynamic relations as discussed in previous section. Length L is the reference length depending on design requirements. All the external/internal oblique shocks are made to meet at a single point so as to obtain maximum capture area and to minimize the spillage losses. This condition is called as *shock on lip* condition and is necessary to avoid unfavorable flow patterns between shocks. The point a_4 is the cowl lip where the external shocks converges. In order to reduce the inlet length, a_4 chosen as the point where the first external oblique shock meets the horizontal line drawn from a_a. Similarly, a_3 is the point where internal shocks converges. The ramp lengths and inlet geometry coordinates are obtained using the trigonometric relations and the derived analytical expressions are given below:

$$x_i = \frac{(\tan(\theta_{i-1}) * x_{i-1}) - (\tan(\beta_i)) * x_{cs} + y_{cs} - y_{i-1}}{(\tan(\theta_{i-1}) - \tan(\beta_i))} \tag{2.5}$$

$$y_i = \tan(\theta_{i-1}) * (x_i - x_{i-1}) + y_{i-1} \tag{2.6}$$

where x_{cs} and y_{cs} is specified as cowl lip coordinates for getting external ramp coordinates and as innerbody shoulder coordinates for internal ramp coordinates respectively.

19

2.3 Scramjet inlet generator

In order to simplify and speed up the design of scramjet inlet geometry generation, there is a need to develop an application which serves this purpose. With this objective, a "scramjet inlet generator" application is developed which takes user inputs such as free stream Mach number and number of internal/external shocks and outputs the profile of the scramjet inlet in a graphical window. The "scramjet inlet generator" (SIG), is an application developed in JAVA and integrated with HTML with an aim to provide an interface to generate scramjet inlets at a specified freestream Mach number. When SIG is executed, it runs the current new design algorithm mentioned in the section. 2.2 in background and outputs the profile of the scramjet inlet.

The advantage of SIG is that it provides a direct interface to design a scramjet inlet and there is a provision to dynamically change the input parameters and see the output accordingly. SIG has a built in x-y plotter is present which obtains its inputs from the code and plots it dynamically. This reduces the inlet design time drastically and provides a user oriented interface to design a scramjet inlet. The SIG can be run on any JAVA supported web browser and this application is combined with GlassFish server interface 3.1.2. This server can be installed in any local computer and SIG application module can be deployed on the server. Once it is deployed, SIG can be launched from any computer connected locally through LAN interface to the host machine. Currently SIG is made to run in a local server, and is accessible from any computer in IIT Hyderabad by just typing the server address in web browser. The screen shot of SIG running in a web browser is shown in Fig. 2.6.

SIG interface is divided into two components, input and output modules. Both the input and output modules exist in the same window. Input module contains various input boxes such as free stream Mach number, number of external shocks, number of internal shocks, specific heat ratio, Mach at cowl, Mach at throat and reference length. The last four parameters are set by default and can be modified by the user requirement. After clicking the "Generate" button, the scramjet inlet profile is generated and is shown in the output module. The output module has a plotting window which outputs the profile of the scramjet inlet in x-y coordinates. Overall total pressure recovery and static pressure of the inlet is shown as an output below the plot window.

Two sample outputs are shown in Fig.2.7 and Fig.2.8 of scramjet inlets generated for Mach 6.5 with 5 external and 5 internal shocks and for Mach 7 with 6 external and 2 internal shocks. Here scramjet inlets are designed to satisfy shock-on-lip condition. The blue line is forebody and the orange is the cowl.
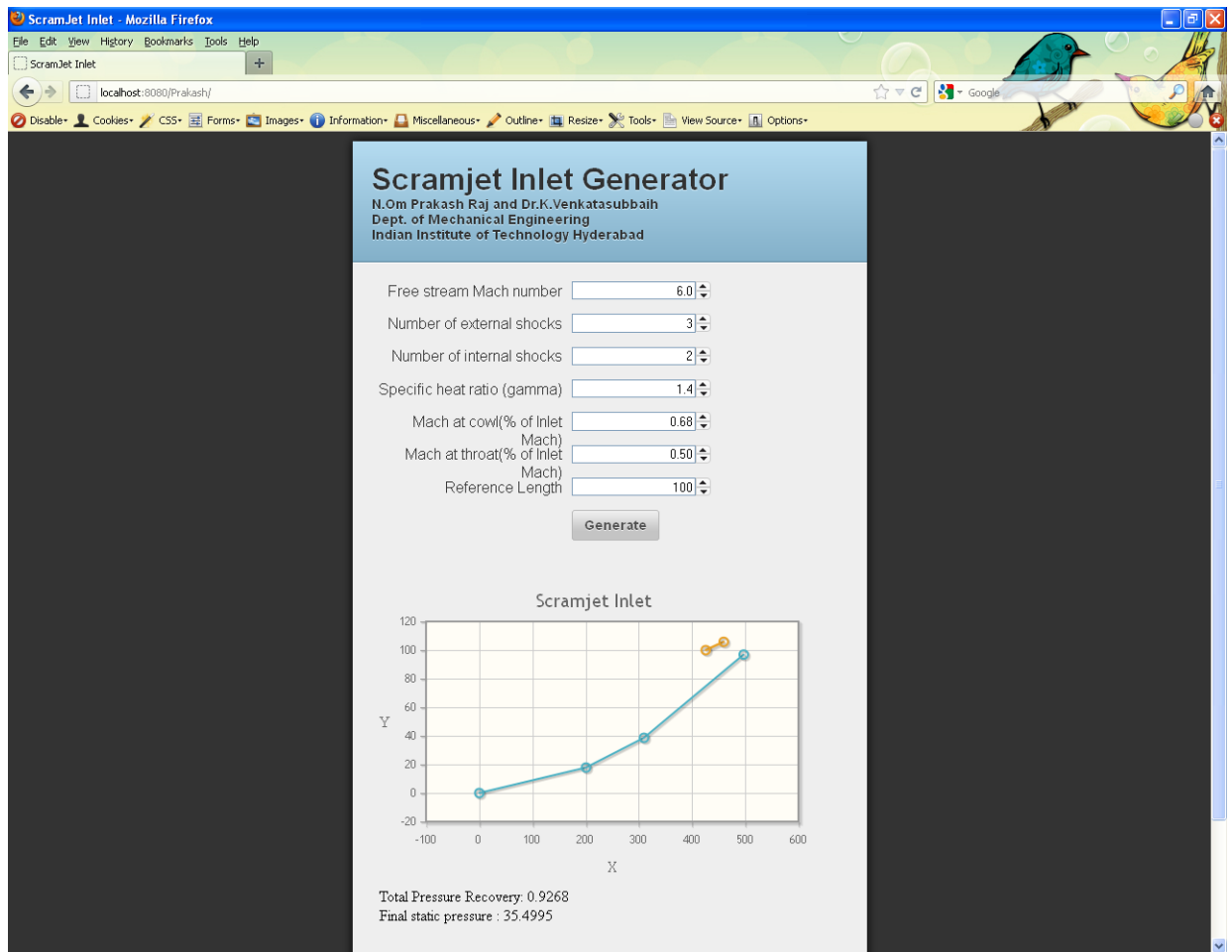
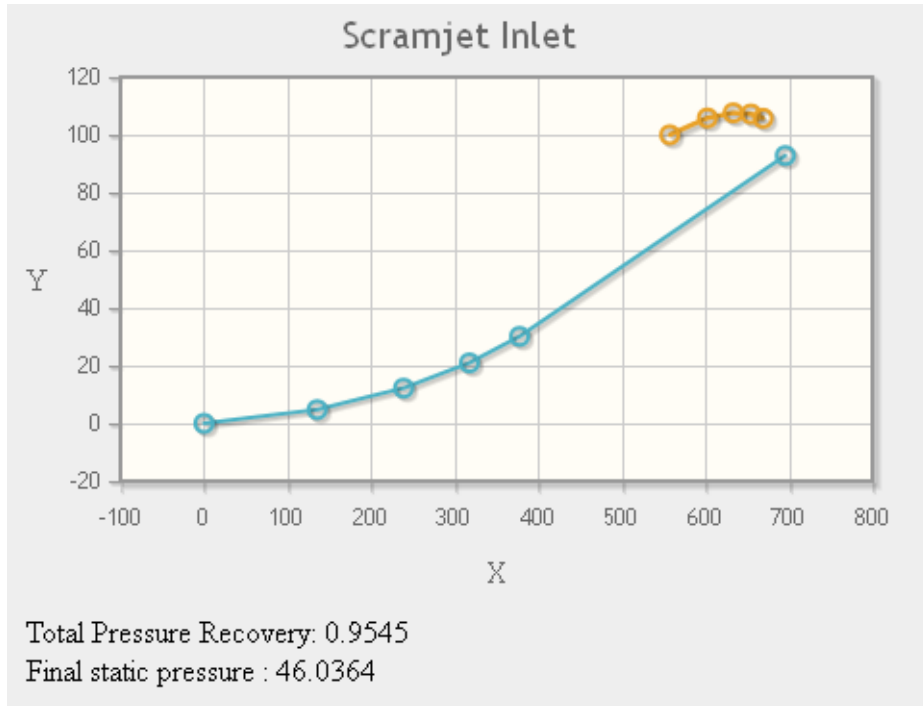Figure 2.6: Screenshot of Scramjet Inlet Generator (SIG)

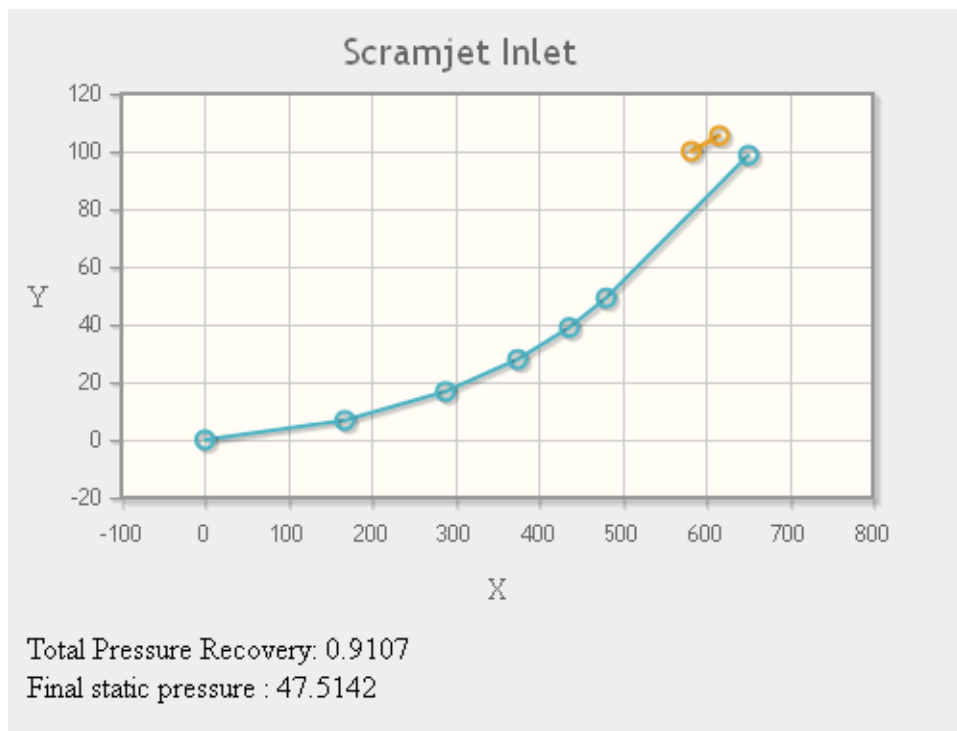Figure 2.7: Scramjet inlet at Mach 6.5 for 5 external and 5 internal shocks generated by SIG

Figure 2.8: Scramjet inlet at Mach 7 for 6 external and 2 internal shocks generated by SIG

2.4 Effect of Mach number on TPR

Total pressure recovery coefficient (TPR) is one of the important performance parameters of scramjet inlet and is defined as the ratio of total pressure at throat to the free stream total pressure or total pressure at isolator exit to the free stream total pressure. The aim of scramjet inlet is to achieve optimum compression and to deliver the compressed fluid into the combustion chamber. Hence, TPR being a measure of compression efficiency is a direct measure of scramjet inlet performance.
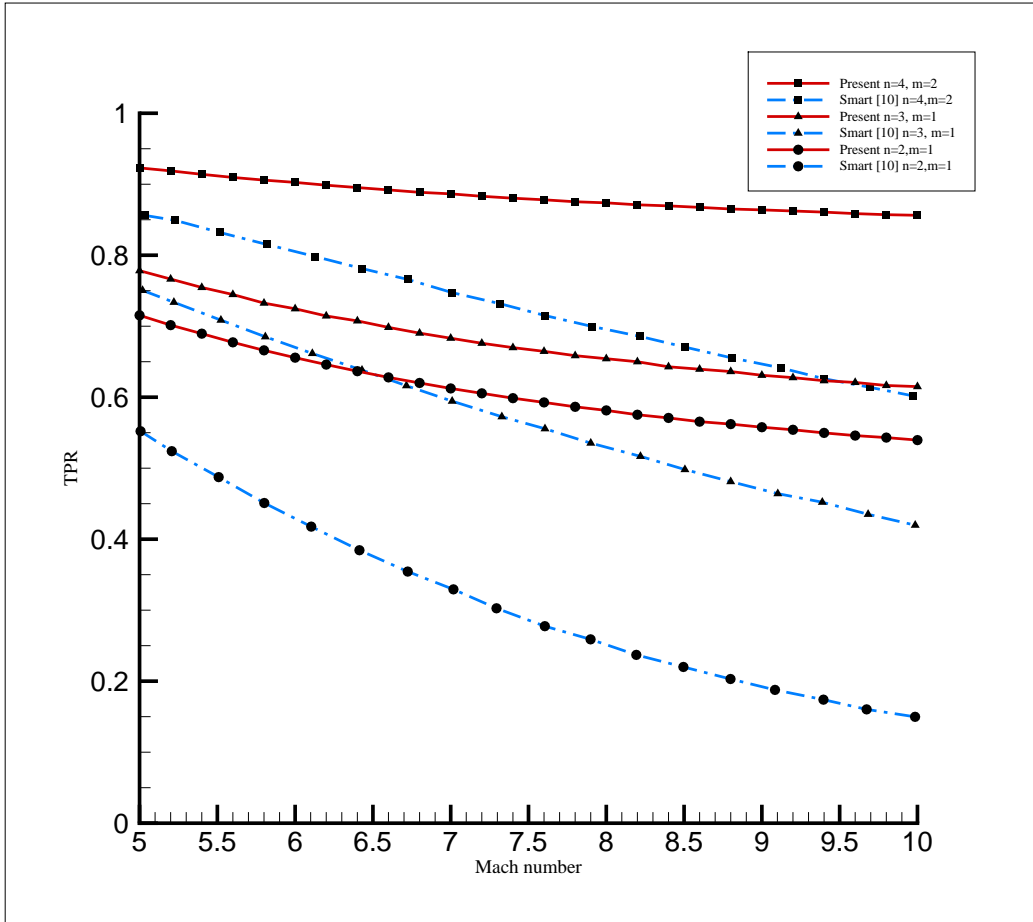

Figure 2.9: Variation of total pressure recovery with Mach number.

Total pressure recovery obtained at different free stream Mach numbers is shown in Figure. 2.9 for different combinations of external and internal shocks. It can be seen from the figure that TPR decreases with an increase in the Mach number and TPR increases with an increase of external or internal shocks due to decrease of shock strength. Present results obtained by the design procedure mentioned in section. 2.2 have been compared with results of Smart [10].The results of Smart [10] were obtained by a design procedure with an approach of optimum total pressure recovery.

Three different combinations of shocks are presented in this Figure. 2.9: 4 external and two internal shocks, 3 external and 1 internal shocks, 2 external and 1 internal shocks. As the number of shocks increases, TPR is found to be increasing. This is due to fact that as the number of shocks are made to be increased, the load on individual shock decreases and hence a single shock has to compress a little, which in turn increases the compression efficiency. From Figure. 2.9, it can be noticed that the present design approach which combines both methodologies of maximizing total pressure recovery and prescribing Mach number at the throat gives a better total pressure recovery when compared to the approach of only maximizing total pressure recovery. This trend is observed even at higher Mach numbers and the deviations observed are significant in the present study and previous approaches in the literature. It can be noted that the current design procedure has better TPR than the previous approach by Smart[10].

2.5   Effect of external/internal shock combinations on turning angles

Fig. 2.10 shows the turning angles obtained at various Mach numbers for different combinations of external and internal shocks i.e. for 2 external and 1 internal, 3 external and 1 internal, 3 external and 2 internal, 4 external and 2 internal shock combinations. In the figure, external shocks angles are represented in red lines and internal shock in green lines. It is evident from the Fig. 2.10 that as the number of shocks increase, angle of turning is found to be decreasing and also when the number of internal shocks are increased, angle of turning required for internal compression also decreased. This is due to the reason that as the number of shocks increase, the shock strength required to turn the flow decreases and this requires small turning angles. Also, as the number of shocks increase, the turning angles decrease and thereby increasing the length of the scramjet intake. There has to be a balance in the number of shocks required and the intake length, so that required flow ratios are obtained for minimal length of the inlet which results in minimal weight of the scramjet inlet. Free stream Mach number has an effect on the turning angles obtained; lower turning angles are obtained as the free stream Mach number is increased.
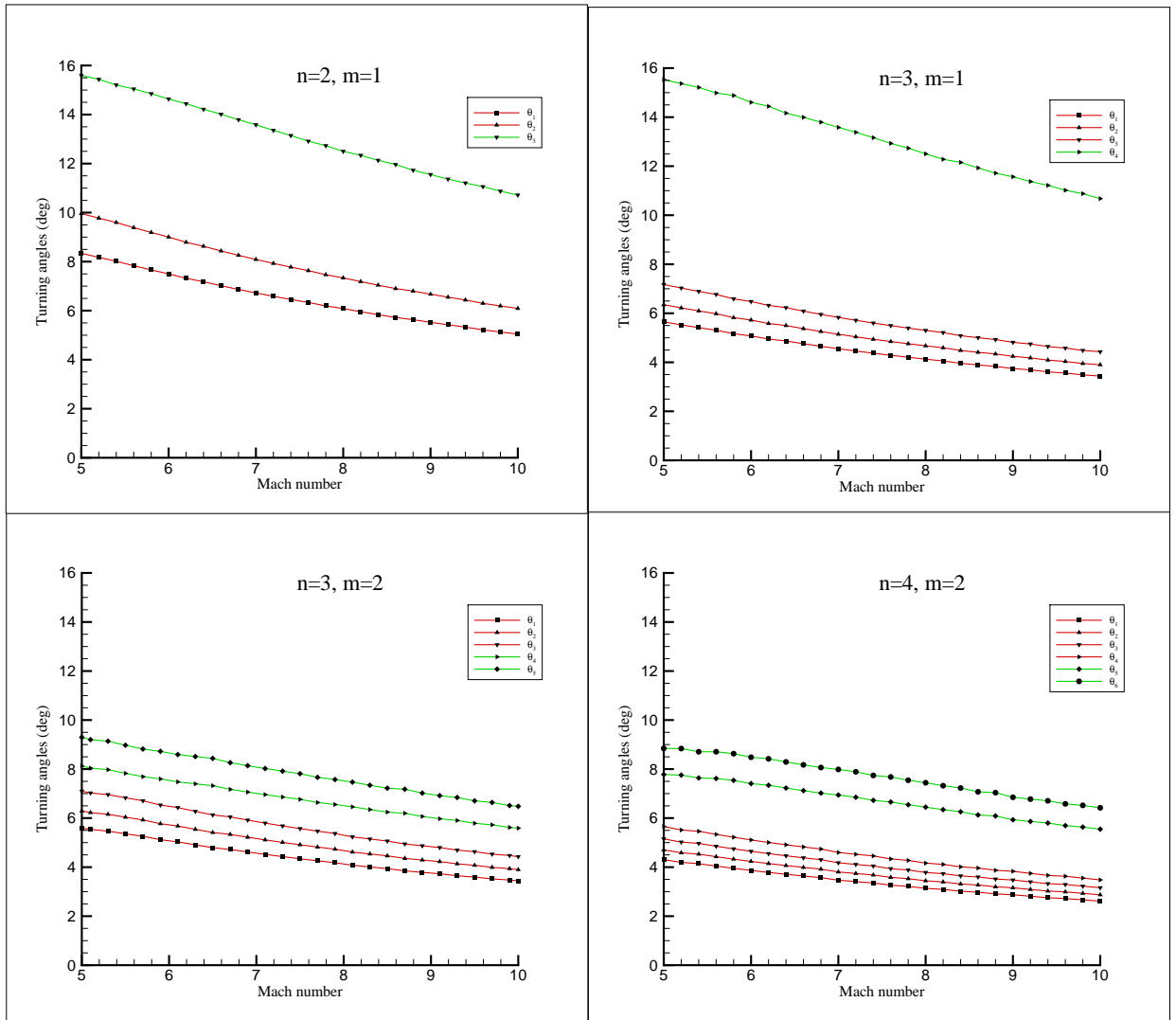
Figure 2.10: Turning angles at various Mach numbers for different combinations of external and internal shocks.

2.6 Effect of M_t and M_e on TPR

Mach number after external compression (M_e) and Mach number at the throat (M_t) are important parameters for design of a scramjet inlet. Both M_e and M_t greatly determine the flow field behavior of the scramjet inlet. Amount of compression required and compression efficiency is dependent on these parameters. In order to know the effects of these parameters on the total pressure recovery, a parametric study is carried out using gas dynamic relations specified in section. 2.2. In this study, M_e and M_t are both varied from 99% of M_0 to 1% of M_0 independently i.e. by fixing M_e and varying M_t from 99% of M_0 to 1% of M_0 or vice-versa. Two Mach numbers are chosen, Mach 5 and Mach 6 and the effects of M_e and M_t on TPR are shown in Fig. 2.11 and Fig. 2.12.
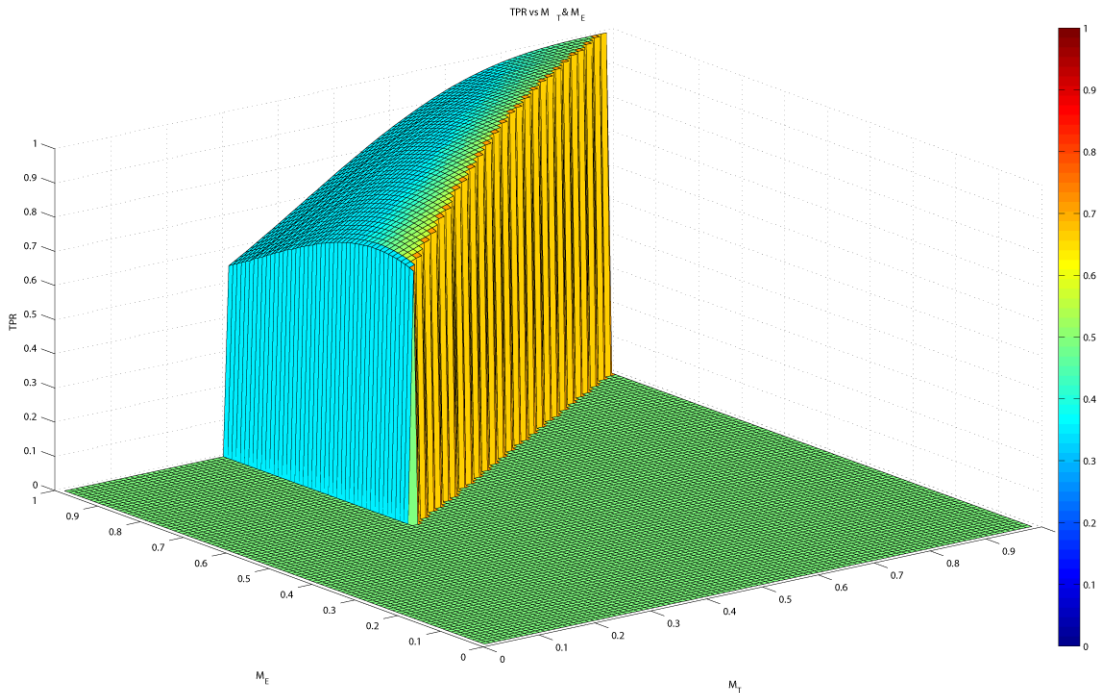

Figure 2.11: TPR vs M_e and M_t for Mach 5.

Fig. 2.11 shows the variation of TPR when M_e and M_t are varied at Mach 5. It is seen from the figure that at a constant M_t, when M_e is varied from 99% of M_0 to 1% of M_0, total pressure recovery is increasing. Here, the TPR has increased as the M_e is decreased and also it after reaching a maximum, TPR starts decreasing and hits no solution zone. The dark green zone indicates no solution zone, where isentropic limit is reached and flow has turned sonic. When different sections of constant M_t are considered, similar trend is observed and TPR increases with increase in M_t. This increase in TPR might be due to the reason that as M_e increases, external shocks have to turn flow lesser and requires low strength shocks and
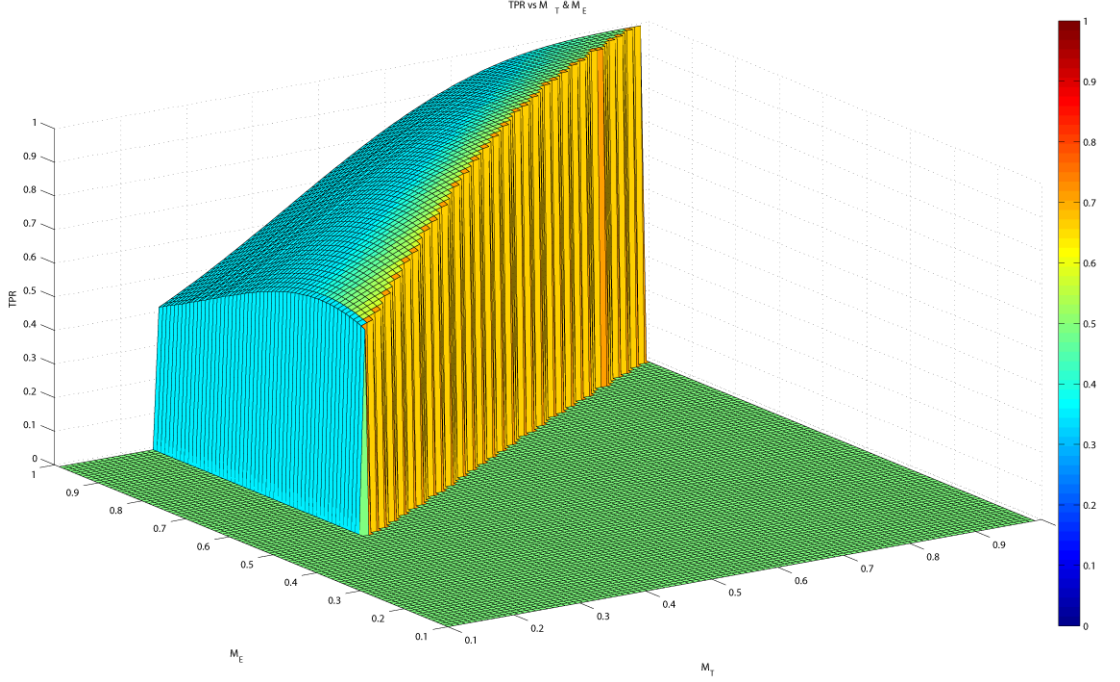
Figure 2.12: TPR vs M_e and M_t for Mach 6.

there by puts additional load on the internal shocks by increasing their shocks strengths. Hence this leads to decrease in total pressure recovery as to the strength of the shock is inversely proportional to the total pressure recovery across the shock. Similar nature as of Mach 5 inlet is observed for Mach 6 scramjet inlet in Fig. 2.12, it can be noted that the range of no solution zone in Mach 6 is comparatively less than Mach 5 in the direction of M_t.

In the current study M_t is specified as 50% of M_0 in order to avoid the formation of separation regions as reported by Mahoney [19]. Fig. 2.13 shows the variation of TPR for different M_e when the throat Mach number is fixed at 50% of M_0 and 40% of M_0 for different Mach numbers. It is seen that when M_t is fixed and M_e is varied from 99% of M_0 to 1% of M_0, it is found that total pressure recovery is maximum for a certain range of Mach numbers. This range varies from 67% of M_0 to 73% of M_0 for $M_t = 50\%$ of M_0 and 65% of M_0 to 71% of M_0 for $M_t = 40\%$ of M_0 at different free stream Mach numbers. Also, M_e cannot be decreased after certain limit as the flow turns sonic, due to occurrence of normal shock and hence no oblique shock solution exists. So in the present design optimum value of $M_e = 68\%$ of M_0 is chosen. Also, when the TPRs of $M_t = 50\%$ of M_0 and $M_t = 40\%$ of M_0 are compared, the TPR range of $M_t = 50\%$ of M_0 is much better than the latter. This is due to the fact that lower Mach number at the throat will force more amount of compression to be done and hence reduces the overall total pressure recovery.
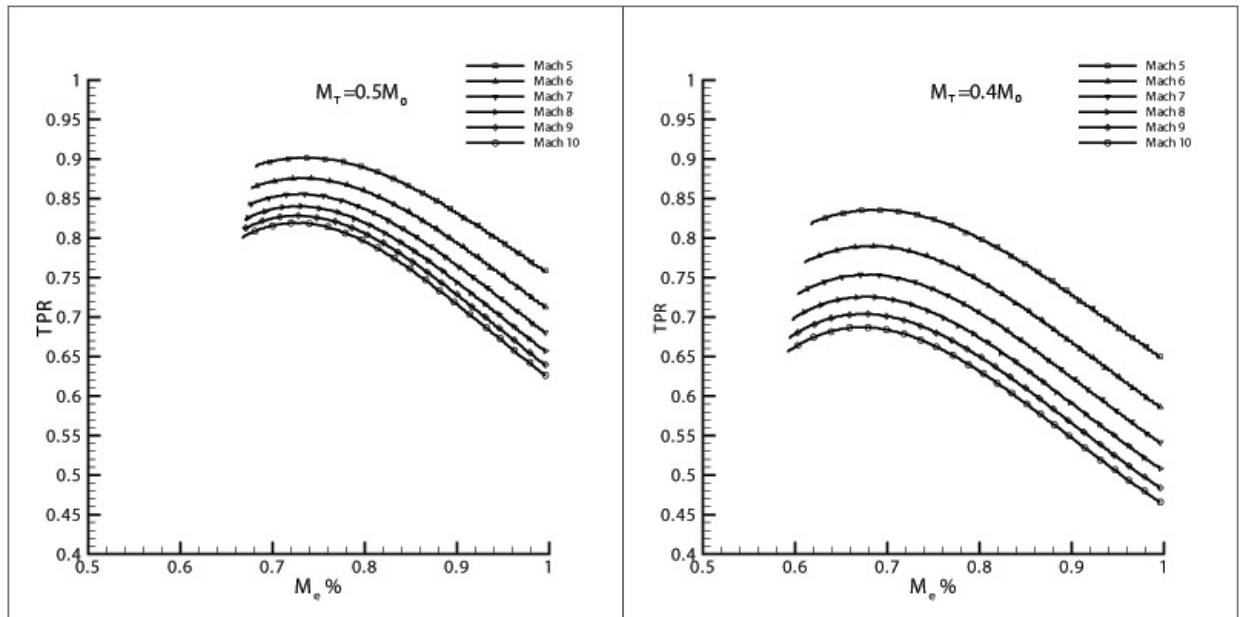
Figure 2.13: Variation of TPR with M_e at throat Mach numbers M_t =50%M_0 and M_t=40%M_0.

2.7   Kantrowitz limit

Inlet is generally unstarted due to over contraction, where the flow chokes or if the back-pressure is raised beyond the level that is sustained by the scramjet inlet. In general, the process of establishing supersonic flow through the scramjet inlet is known as inlet start-ing. Contraction ratio is defined as the ratio of cross sectional area at the cowl to the throat. For hypersonic inlets, internal contraction ratio has significant effect on the inlet starting operation. However, by employing variable geometry intakes, starting problem can be avoided but this adds to overall weight of the system and decreases the performance of the scramjet engine. A theoretical starting limit known as Kantrowitz limit exists to put a limit on the internal contraction ratios. Developed by Kantrowitz and Donaldson [16], it gives the limiting contraction ratio for a diffuser until after which the inlet chokes.

Fig. 2.14 shows the Kantrowitz limit for various Mach numbers at cowl i.e. Mach num-ber after external compression along with the present contraction ratios of inlet geometries. Contraction ratios higher than the Kantrowitz limit are desirable to avoid the inlet unstart as reported by Curran and Murthy[6]. Present contraction ratios of inlet geometries are higher than the Kantrowitz limit. This indicates that current design satisfies the Kantrowitz limit and scramjet inlets designed by this procedure will avoid unstart problem without even using the variable geometry.
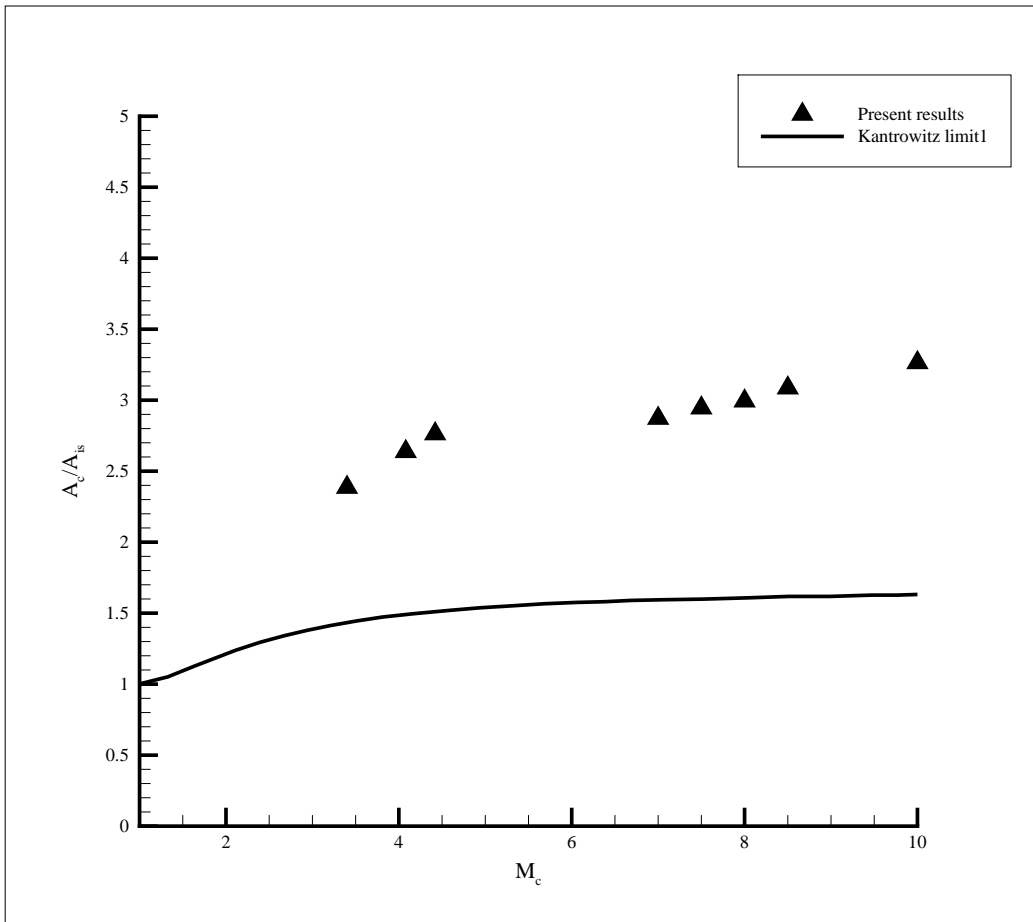
28

Figure 2.14: Variation of contraction ratio at different Mach numbers.

Chapter 3

Numerical analysis of scramjet inlets

3.1 Governing equations

The governing equations are derived from conservation laws and the second law of thermo-dynamics. The conservation equations for turbulent compressible flows are as follows:

Continuity equation:
Conservation of mass states that the total mass of the universe is constant; in other words, mass is neither created nor destroyed but can only be moved from one place to another.

$$\frac{\partial \rho}{\partial t} + \frac{\partial}{\partial x_j} [\rho u_j] = 0, \quad j = 1, 2, 3 \tag{3.1}$$

Momentum equation:
Conservation of momentum says that momentum changes due to one of three factors - redistribution, conversion of momentum to or from energy, and force. In other words, if momentum increases in one place, either momentum or an equivalent amount of energy must decrease someplace else, or a force must act.

$$\frac{\partial}{\partial t} (\rho u_i) + \frac{\partial}{\partial x_j} [\rho u_i u_j + p \delta_{ij} - \tau_{ji}] = 0, \quad i, j = 1, 2, 3 \tag{3.2}$$

Energy equation:
Conservation of energy says that energy change is due to one of three factors redistribution, conversion of energy to or from momentum, or conversion to or from some other form of

energy, heat, or work. In other words, if energy increases in one place, either energy or an equivalent amount of momentum must decrease someplace else, or heating or work must be done.

$$\frac{\partial}{\partial t}\left(\rho e_0\right) + \frac{\partial}{\partial x_j}\left[\rho u_j e_0 + u_j p + q_j - u_i \tau_{ij}\right] = 0, \quad i, j = 1, 2, 3 \tag{3.3}$$

Viscous stress is given by:

$$\tau_{ij} = 2\mu S_{ij}^*, \quad i, j = 1, 2, 3 \tag{3.4}$$

Where the viscous strain rate is defined by,

$$S_{ij}^* \equiv \frac{1}{2}\left(\frac{\partial u_i}{\partial x_j} + \frac{\partial u_j}{\partial x_i}\right) - \frac{1}{3}\frac{\partial u_k}{\partial x_k}\delta_{ij}, \quad i, j = 1, 2, 3 \tag{3.5}$$

Where $\mu = \mu_l + \mu_t$ is the total viscosity; μ_l, μ_t being the laminar and turbulent viscosity

Laminar viscosity (μ_l) is calculated from Sutherland's law as

$$\mu_l = \mu_{ref}\left(\frac{T}{T_{ref}}\right)^{3/2}\frac{T_{ref} + S}{T + S} \tag{3.6}$$

T_{ref} is a reference temperature.
μ_{ref} is the viscosity at the T_{ref} reference temperature
S is the Sutherlands coefficient

Specific heat as a function of temperature is given by,
For $300 <= T < 1000$

$$c_p(T) = 429.929 + 1.784T - 1.966 * 10^{-3}T^2 + 1.297 * 10^{-}6T^3 - 4.000 * 10^{-10}T^4$$

For $1000 <= T < 5000$

$$c_p(T) = 841.377 + 0.593T - 2.415 * 10^{-4}T^2 + 4.523 * 10^{-8}T^3 - 3.153 * 10^{-12}T^4$$

And,

$$\gamma \equiv \frac{C_p}{C_v}$$
$$p = \rho R T$$

The RNG-based k-ϵ turbulence model is derived from the instantaneous Navier-Stokes equations, using a mathematical technique called "renormalization group" (RNG) methods. This model is more accurate and reliable for a wider class of flows than the standard k-ϵ model.

Turbulent transport equations of $k - \epsilon$ model with Re-Normalisation Group (RNG) are given by,

Turbulent kinetic energy equation:

$$\frac{\partial}{\partial t}(\rho k) + \frac{\partial}{\partial x_i}(\rho k u_i) = \frac{\partial}{\partial x_j}\left[\left(\mu + \frac{\mu_t}{\sigma_k}\right)\frac{\partial k}{\partial x_j}\right] + P_k - \rho\epsilon \tag{3.7}$$

Turbulent dissipation rate equation:

$$\frac{\partial}{\partial t}(\rho \epsilon) + \frac{\partial}{\partial x_i}(\rho \epsilon u_i) = \frac{\partial}{\partial x_j}\left[\left(\mu + \frac{\mu_t}{\sigma_\epsilon}\right)\frac{\partial \epsilon}{\partial x_j}\right] + C_{1\epsilon}\frac{\epsilon}{k}P_k - C_{2\epsilon}^*\rho\frac{\epsilon^2}{k} \tag{3.8}$$

Where

$$C_{2\epsilon}^* = C_{2\epsilon} + \frac{C_\mu \eta^3(1-\eta/\eta_0)}{1+\beta\eta^3}$$
$$\text{And } \eta = Sk/\epsilon \text{ , } S = (2S_{ij}S_{ij})^{1/2}$$

Turbulent viscosity is given by,

$$\mu_t = \rho C_\mu \frac{k^2}{\epsilon} \tag{3.9}$$

And the corresponding constants are:

$$C_\mu = 0.0845$$
$$\sigma_k = 0.7194$$
$$\sigma_\epsilon = 0.7194$$
$$C_{\epsilon 1} = 1.42$$
$$C_{\epsilon 2} = 1.68$$
$$\eta_0 = 4.38$$

32

3.2   Numerical method

Two dimensional unsteady compressible turbulent flow equations are solved using commercial CFD software FLUENT. Kinetic energy (k)-turbulent dissipation (ϵ) model with renormalization group is implemented for modeling turbulence. Air is considered as an ideal gas with variable properties. Sutherlands law is used to calculate the viscosity and piecewise polynomial is used to calculate temperature dependent specific heat. The boundary conditions at the inflow are specified as free stream operating conditions and the flow variables at the outflow are extrapolated from the interior. No-slip boundary conditions are imposed at the solid walls for velocity field. Adiabatic boundary condition is used to obtain a maximum surface temperature on scramjet inlet and a constant surface temperature condition is used for other cases. A fine grid is used in the isolator section to capture the shock-shock and shock/boundary layer interactions.

Pre-processing

Pre-processing is divided into two stages Geometry and Meshing. It is carried out using ANSYS ICEM CFD 13.0. The geometric details of Mach 10.4 inlet obtained from Van Wie and Ault [25] are used to model the geometry (other geometrical details of scramjet inlets mentioned in this study are obtained using Section.2.2). After the geometry is modeled using ANSYS ICEM CFD 13.0, stage two i.e. meshing is carried out. By using a blocking strategy, geometry is split into several blocks upon which a rectangular mesh is generated. Different stages of blocking for Mach 10.4 geometry is shown in Fig. 3.1. From Fig. 3.1, stage 1 shows the geometry and 2D planar blocking is initialized in stage 2. A rectangular block is generated over the inlet geometry in stage 2 and this has to be wrapped over the geometry. In stage 3, the rectangular block is split into several blocks by using split block operation. Vertices of the blocks are associated to the inlet geometry by using association tools and this is done until the blocks form the shape of the inlet geometry and this is shown in stage 4. Finally in stage 5, mesh is computed on the geometry. For viewability, a very coarse mesh is shown in stage 5 of Fig. 3.1.
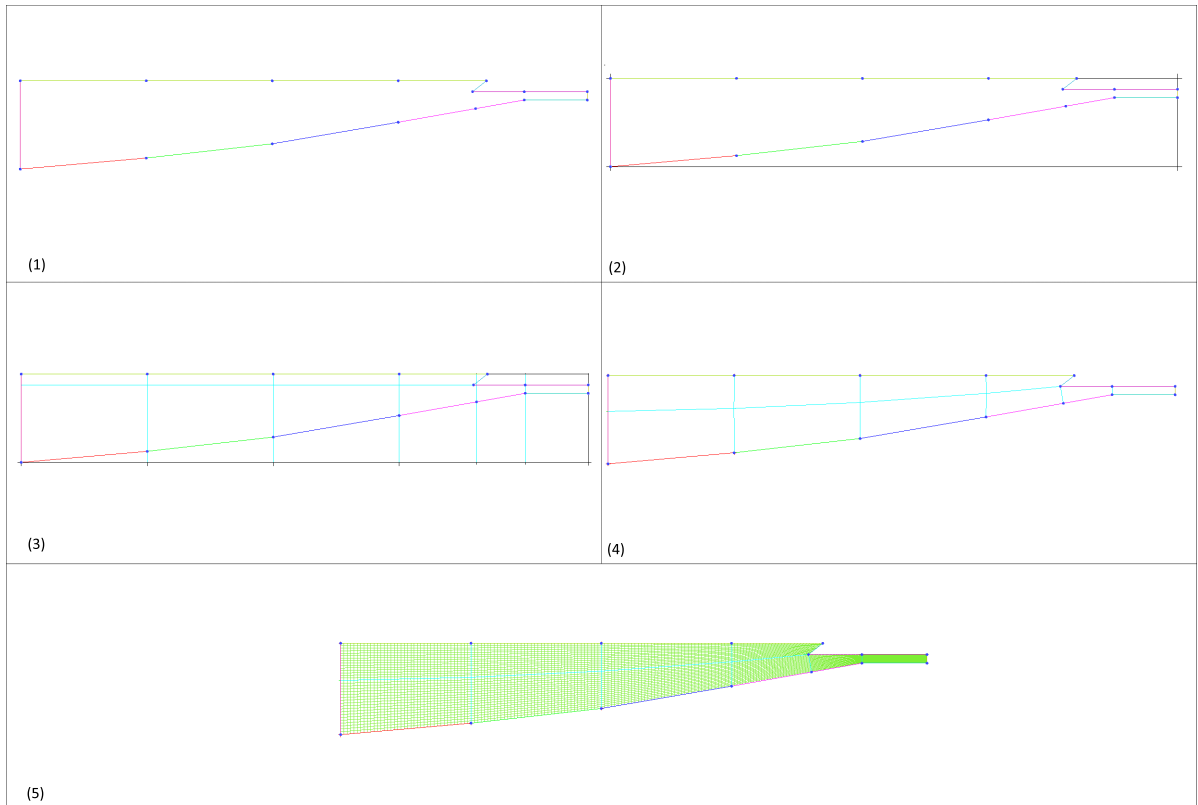
Figure 3.1: Pre-processing stages for Mach 10.4 geometry.

Mesh generated for Mach 10.4 geometry is shown in Fig. 3.2. Fine grid is created in the isolator section to capture shock-shock and shock/boundary layer interactions efficiently. 30 times zoomed portion of mesh in isolator region is shown in Fig. 3.3. Three different meshes were made coarse, medium and fine of 75969 cells, 184659 cells and 305100 cells respectively.
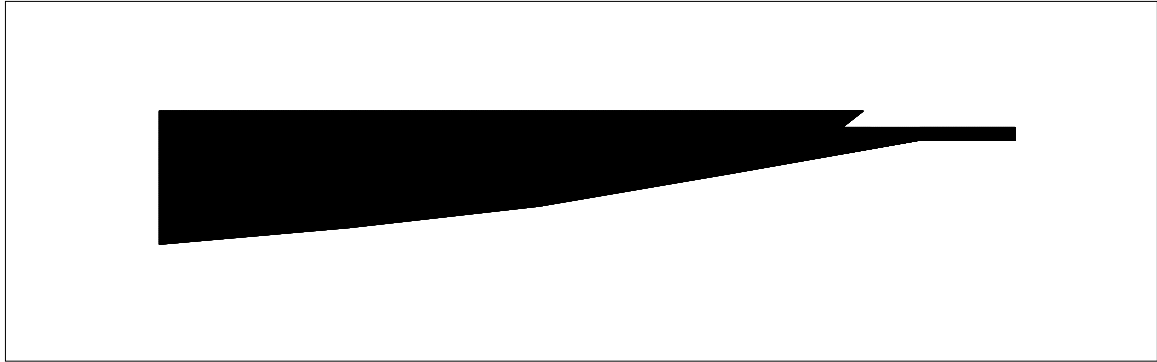

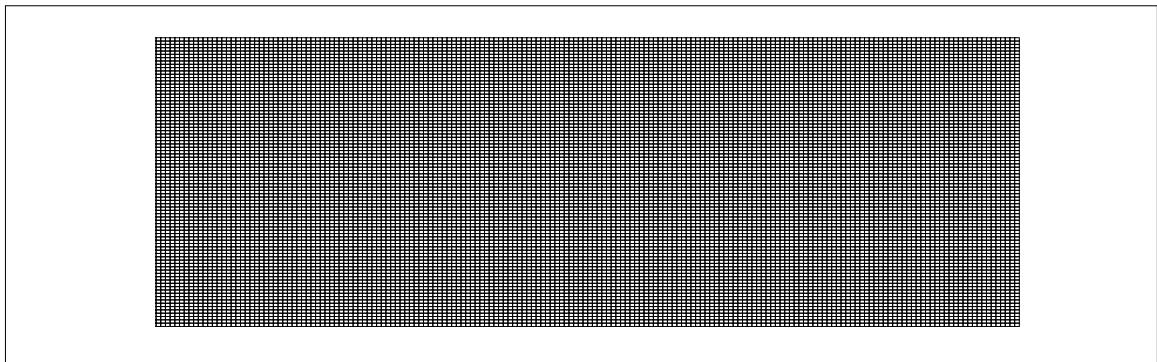Figure 3.2: Geometry and Mesh of Mach 10.4 inlet.

Figure 3.3: 30X Zoomed mesh in isolator region of Mach 10.4 inlet.

3.3   Validation study

3.3.1   Inlet model

The purpose of scramjet inlet is to provide supersonic air flow to the combustion process. The scramjet inlet consists of three parts namely forebody, cowl and innerbody as shown in Fig. 3.4. External compression shocks originate from the forebody and internal compression process takes place between the cowl and innerbody. Innerbody starts at the end of forebody and cowl starts from the cowl tip. Both innerbody and cowl extends to the inlet of combustion chamber. Isolator is the horizontal section between cowl and innerbody. The schematic diagram of scramjet inlet is shown in Fig. 3.4 for Mach 10.4. The geometrical parameters of inlet at Mach 10.4 are taken from Van Wie and Ault [25] and are given in Table. 3.1. The compression angle of the two external shocks is 5^0 for Mach 10.4 inlet. It is specified by Van Wie and Ault [25] that Mach 10.4 inlet is designed at Mach 20 i.e. it satisfies *shock-on-lip* condition for Mach 20 but is operated at Mach 10.4.
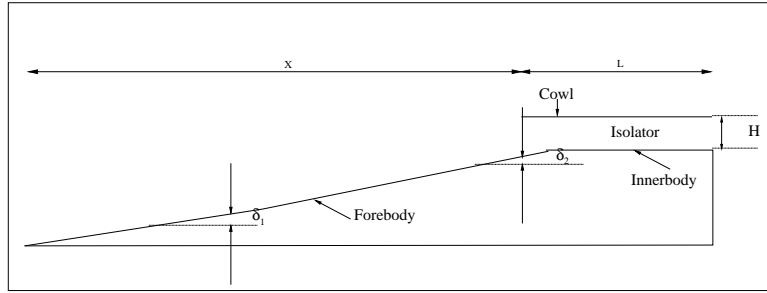

Figure 3.4: Geometry of Mach 10.4 inlet.

Table 3.1: Geometrical parameters for Mach 10.4 inlet.

	X	L	H
Length (m)	0.9144	0.22 86	0.0168
	δ_1	δ_2	
Angle (deg)	5	10	

3.3.2 Grid independency test

Three different mesh sizes have been simulated for Mach 10.4 at operating conditions of Mach number $M_0 = 10.4$, static pressure $P_0 = 75647.65$ Pascal, $T_0 = 215K$ and with a constant surface temperature of $T_w = 1000K$. Surface static pressure distribution along forebody is plotted for different mesh sizes in Fig. 3.5. Quantitative comparison of various mass-weighted averaged performance parameters at isolator exit at three different grid sizes of coarse mesh 75969 cells, medium mesh 184659 cells and fine mesh 305100 cells are given in Table. 3.2. It can be seen that solution is grid independent and there is very less variation in the performance parameters for coarse, medium and fine mesh sizes. Hence, medium mesh is chosen for all the simulations reported henceforth. Convergence of 10^{-4} for continuity and momentum and 10^{-6} for K and ϵ is satisfied and additional convergence of mass imbalance less than 0.1% is imposed.
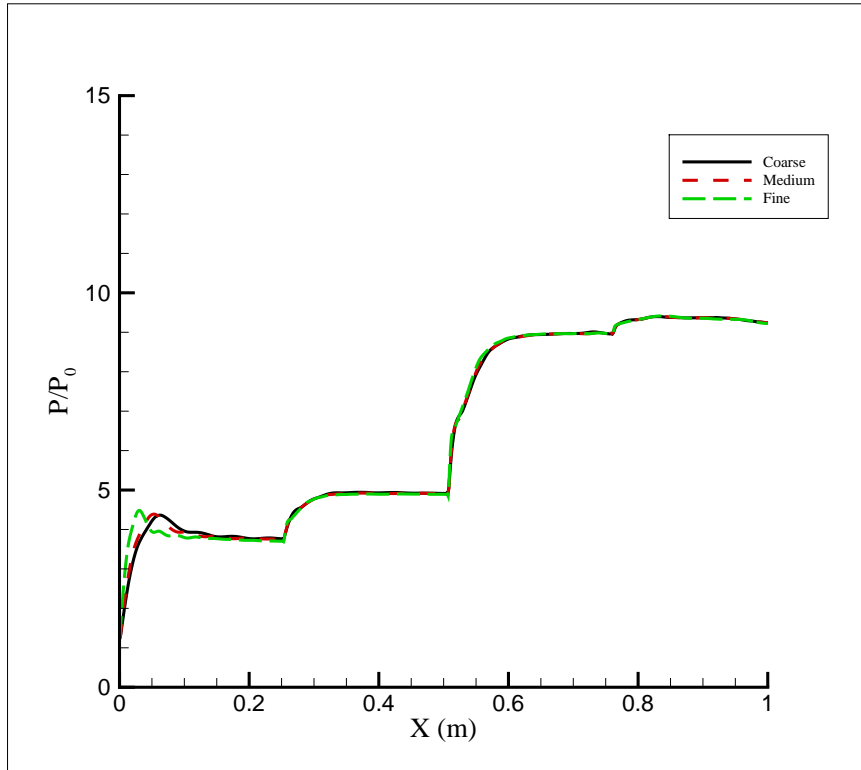

Figure 3.5: Grid independency test on forebody pressure distribution.

Table 3.2: Comparison of different parameters at various grid levels.

Grid	P_{exit}/P_0	$P_{t_{exit}}/P_{t_0}$	M_{exit}
Coarse	34.659	0.428	5.07
Medium	34.682	0.433	5.09
Fine	34.779	0.445	5.11

3.3.3 Comparison of experimental and CFD results

Study of scramjet inlet flow field involves the complex phenomenon of inviscid/viscous coupling, shock-shock interactions, shock/boundary layer interactions, separation etc. Computational fluid dynamics (CFD) being one of the most powerful tools for understanding various flow phenomena and helps in analyzing the flow field physics and helps in designing and analysis of the scramjet inlet. The scramjet inlet geometry for Mach 10.4 has been analyzed using CFD and reported here. The accuracy of present numerical methods is confirmed by validating current results with the experimental results available in the literature Van Wie and Ault [25]. Mach 10.4 inlet flow field characteristics are obtained with free stream conditions of Mach number $M_0 = 10.4$, static pressure $P_0 = 75647.65$ Pascal, free stream temperature $T_0 = 215K$ and walls with a constant surface temperature $T_w = 1000K$. Surface static pressure distribution along the forebody, cowl and inner body plotted in Figure. 3.6. Experimental data is shown in discrete symbols and present results are shown in solid lines. Surface static pressure along the forebody is increasing due to external compression shocks. Sudden deviations in pressure on cowl and innerbody at the start of isolator section are due to impingement of cowl shock on the innerbody shoulder. Present results showed an excellent agreement with experimental results of Van Wie and Ault [25].

Density contours of Mach 10.4 inlet of are shown in Fig. 3.7. Experimental Schileren image is taken from Van Wie and Ault[25] for the above mentioned operating conditions and has been shown here to compare the same with current CFD results. The experimental results are plotted in Fig. 3.7 (a) and in Fig. 3.7 (b). The current contours are in agreement with the experimental contours.

Pressure, density and Mach number contours are shown in Fig. 3.8 for Mach 10.4 inlet. In Fig. 3.8, contours are plotted at quasi steady state condition i.e. when the solution is not changing with increase in time. Formation of oblique shocks and boundary layer near the forebody are shown in Fig. 3.8. Oblique shocks originate along the forebody and the fluid gets compressed as it passes through the shocks and is directed into the isolator region. The scramjet inlet of Van Wie and Ault[25] is designed for Mach 20 but is operated below design condition i.e. at Mach 10.4 and hence shock-on-lip condition is not satisfied in this case.
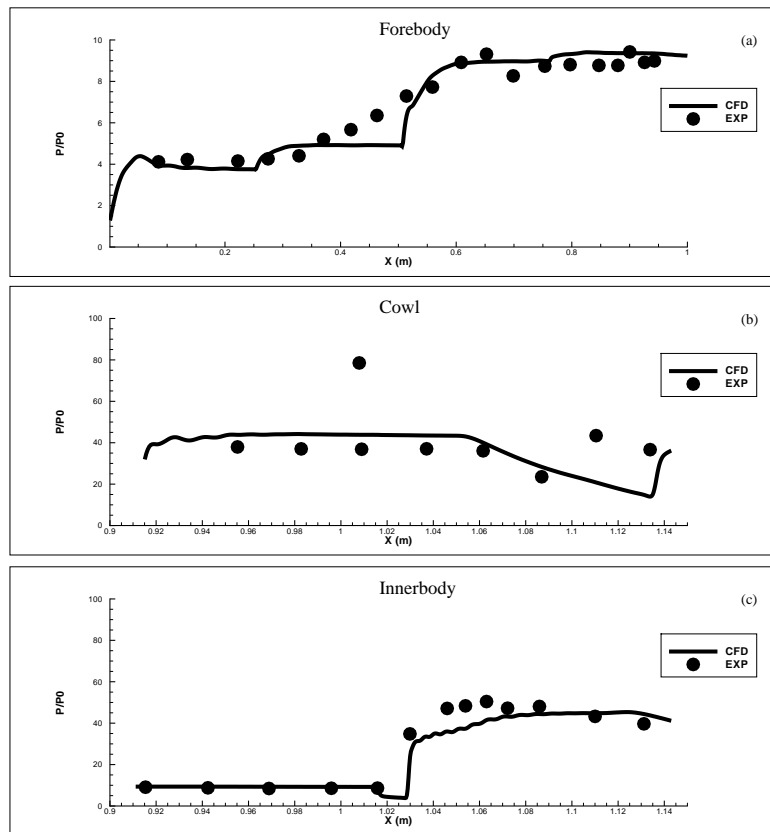
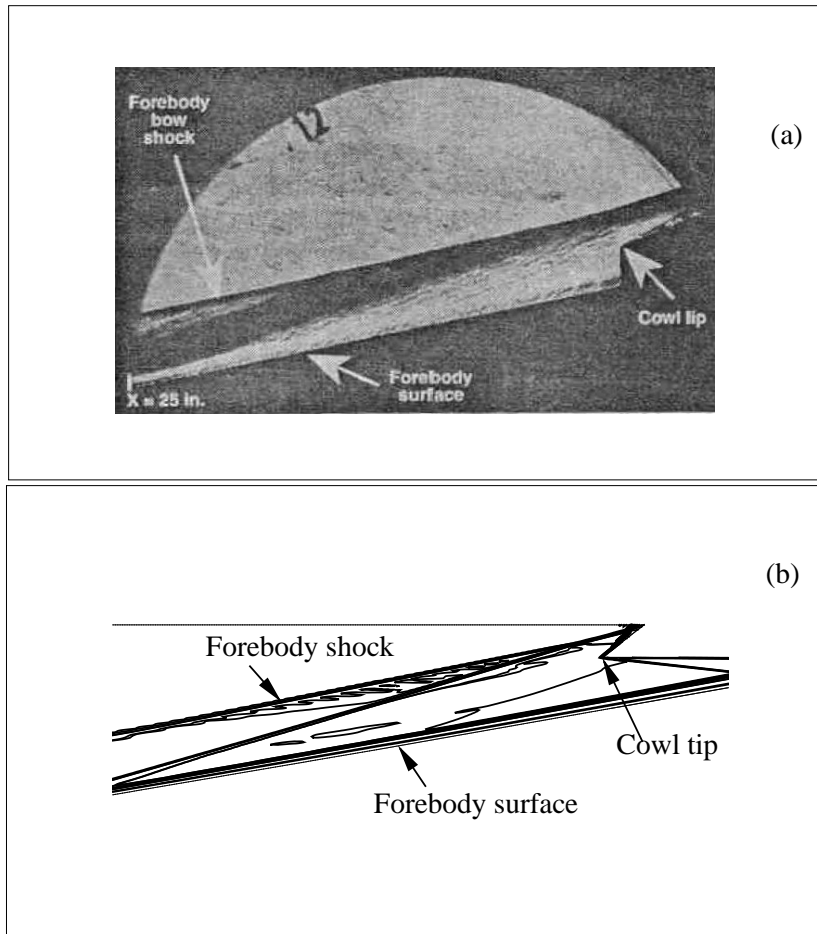Figure 3.6: Pressure distribution along the surface of scramjet inlet.

Figure 3.7: Comparison of (a) Schilerin image of Van Wie and Ault [25] (b) density contours of current CFD study.
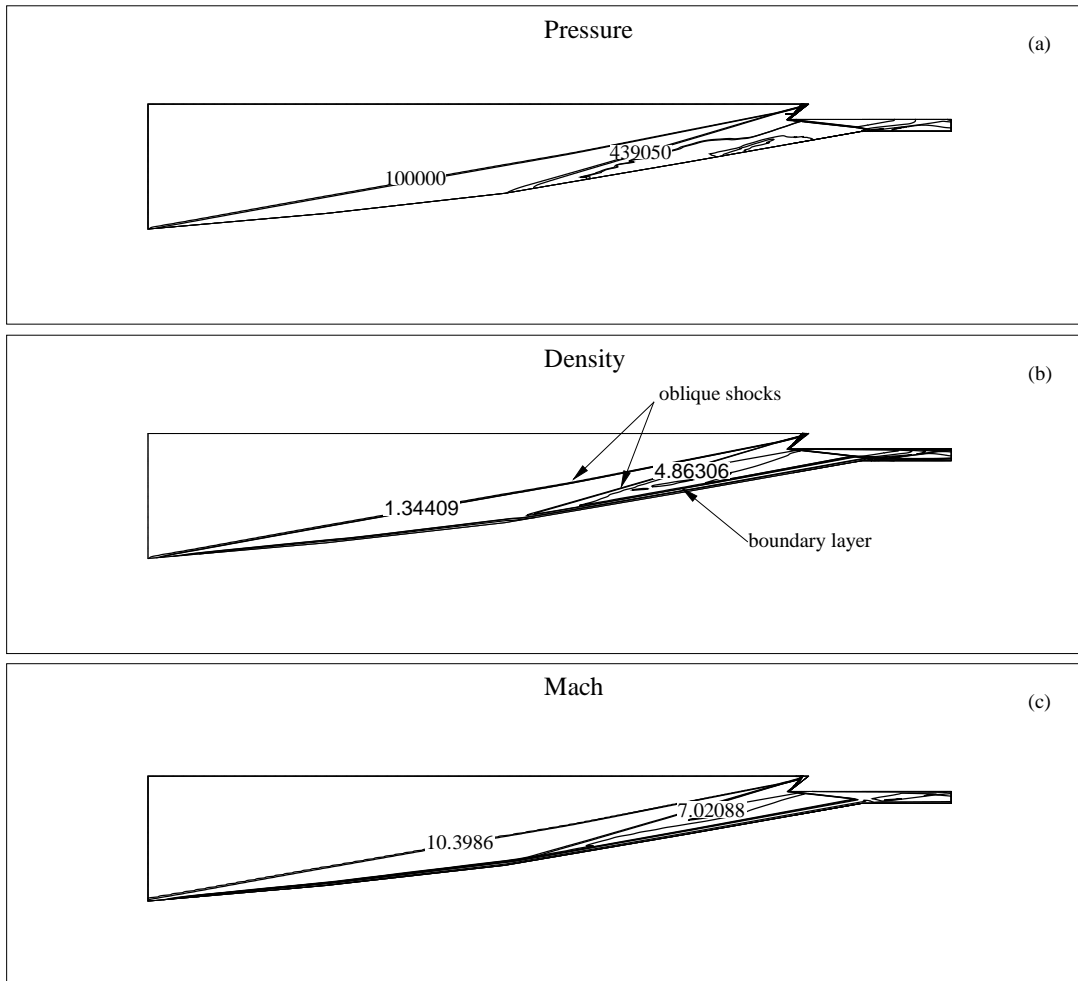
Figure 3.8: Contours of (a) Pressure (b) Density and (c) Mach for Mach 10.4 inlet.

3.4 Inviscid and Viscous effects

The design methodology in section. 2.2 uses 1D gas dynamic relations to obtain the geometry. Current approach aims to make the inlet geometry satisfy the *shock-on-lip* condition, but this is done by only using 1D gas dynamic relations which involves many approximations. Hence, it is required to check whether the *shock-on-lip* condition is satisfied or not when inviscid and viscous effects are considered. There might also be deviations in in the performance parameters obtained when the aforementioned effects are considered. Hence, CFD simulations are carried out on various inlet geometries to find out the effects on inviscid and viscous effects on the scramjet inlet and to verify the *shock-on-lip* condition. All the geometries mentioned are simulated with free stream conditions of static pressure $P_0 = 6079.5$ Pascal, free stream temperature $T_0 = 230K$ and walls with a constant temperature of $T_w = 1000K$. Unless otherwise stated, 3 external shocks and 2 internal shocks is the criterion and only the above operating conditions are only used in the preceding sections.

3.4.1 Mach 6 inlet

Mach 6 inlet geometry that is generated by current design procedure is simulated and the flow field characteristics are obtained with the free stream conditions mentioned previously. Isolator length is chosen as the ten times the width of the throat. Pressure contours are shown in Fig. 3.9 and Fig. 3.10 for the inviscid case and viscous case respectively for Mach 6 geometry. The contours are plotted at quasi-steady state condition i.e. when the solution is not changing with increase in time. Tecplot 360 is used for post processing the data and all units are in SI system.
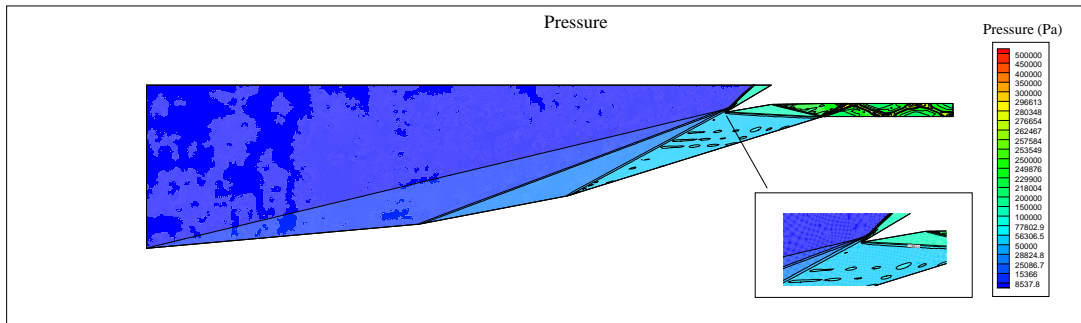

Figure 3.9: Pressure contours of Mach 6 geometry (Inviscid case).

From Fig. 3.9 and Fig. 3.10 it is seen that, external compression shocks are originating from the forebody and the internal compression shocks are originating from the cowl. Isolator section consists of series of multiple shock reflections started by the cowl shocks impinging on the innerbody. Zoomed contours of pressure near the cowl are also given in the
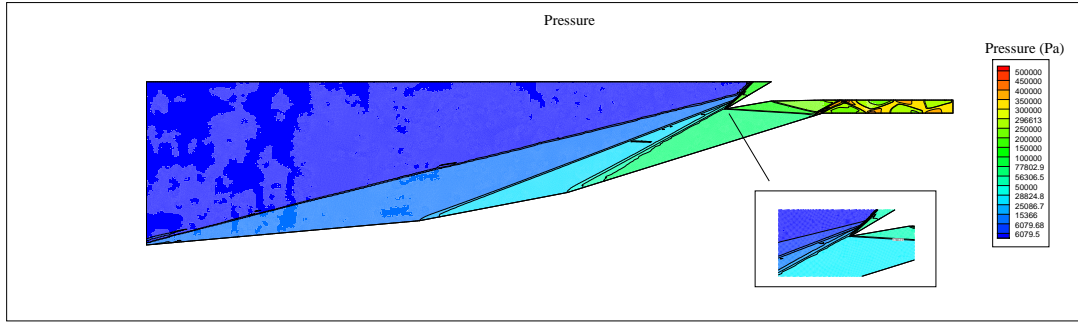
Figure 3.10: Pressure contours of Mach 6 geometry (Viscous case).

same figures which show the position of external shocks from the forebody. It is clearly seen from the inviscid and viscous pressure contours that *shock-on-lip* condition is not satisfied. As the design procedure used 1D gas dynamic relations which itself has many approximations, the geometry doesn't satisfy *shock-on-lip* condition when these effects are considered. From Fig. 3.10, the deviation from the design condition in viscous case is greater than that of inviscid case. Hence, it can be said that as Mach 6 inlet geometry doesn't satisfy *shock-on-lip* condition, design Mach number of Mach 6 inlet geometry is not Mach 6 but some another Mach number.

As the inlet geometry has not satisfied the imposed *shock-on-lip* condition, the inlet geometry is simulated at a higher Mach number to check whether it satisfies *shock-on-lip* condition. The inlet geometry is simulated at Mach 6.5 for inviscid and viscous effects and the contours of pressure, density and Mach are shown in Fig. 3.11 for viscous case. From Fig. 3.11, it is seen that the *shock-on-lip* condition is satisfied. This shows that the design Mach number of Mach 6 geometry is Mach 6.5.

Performance parameters such as static pressure ratio, total pressure recovery (TPR) and Mach number are evaluated at throat and at the isolator exit for Mach 6 inlet geometry for 1D inviscid, 2D inviscid and viscous effects and are given in Table. 3.3. Here, throat is defined as the region where the isolator section begins. From Table. 3.3 the TPR at the throat has decreased from 0.864 to 0.825 when two dimensional effects are considered, which shows that two dimensional effects have to be considered for the design of scramjet inlet. It can be noticed that TPR has further decreased from throat to the isolator exit. Even though TPR has decreased in the isolator, it is needed to avoid the back pressures entering from the combustion chamber to the inlet.
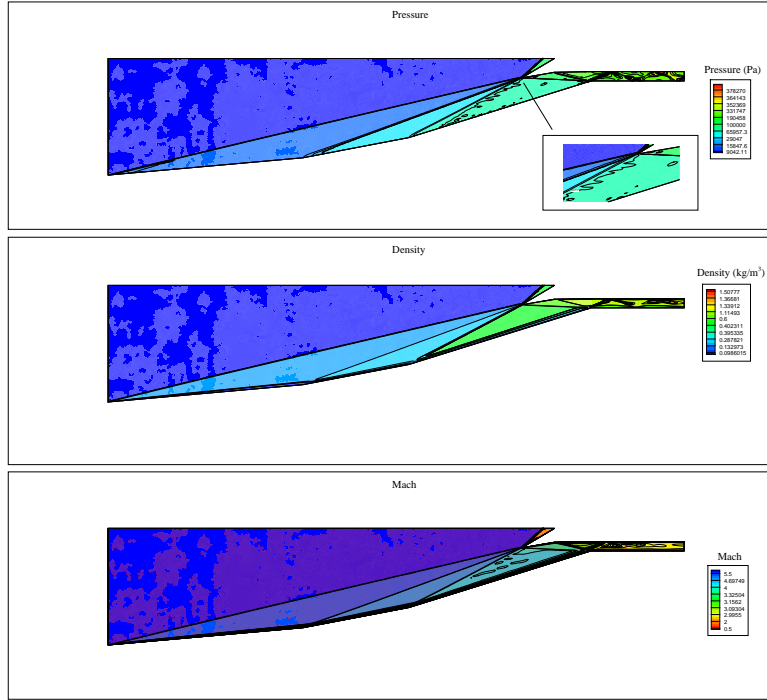
Figure 3.11: Contours of Mach 6 geometry simulated at Mach 6.5 (Viscous case).

Table 3.3: Performance parameters of Mach 6 inlet geometry for 1D, 2D, inviscid and viscous effects

Mach	6(1D Inviscid)	6(2D Inviscid)	6(Viscous)	6.5(2D Inviscid)	6.5(Viscous)
SPR_{throat}	35.49	39.81	48.23	45.06	50.8
TPR_{throat}	0.864	0.825	0.684	0.75	0.675
M_{throat}	3	2.94	2.67	3.14	2.94
SPR_{exit}	-	40.272	51.506	44.69	56.046
TPR_{exit}	-	0.8105	0.5107	0.73	0.5277
M_{exit}	-	2.9251	2.45	3.124	2.726

3.4.2 Mach 8 inlet

Mach 8 inlet geometry generated by the design procedure specified in section. 2.2 is simulated at two different free stream Mach numbers Mach 8, 9. The behavior of *shock-on-lip* condition and the inviscid and viscous effects on various performance parameters are reported. Pressure contours of Mach 8 geometry operated at Mach 8 for inviscid and viscous cases are given in Fig. 3.12and Fig. 3.13. It is found from the contours that the *shock-on-lip* condition is not satisfied at Mach 8 and hence the design Mach number for the Mach 8 inlet geometry is not Mach 8. This same inlet geometry is simulated at higher Mach numbers and found that *shock-on-lip* condition is satisfied at Mach 9 and hence the design Mach number is found to be at Mach 9. Contours of pressure, density and Mach are shown in Fig. 3.14 for Mach 8 inlet geometry which is simulated at Mach 9 for viscous effects.
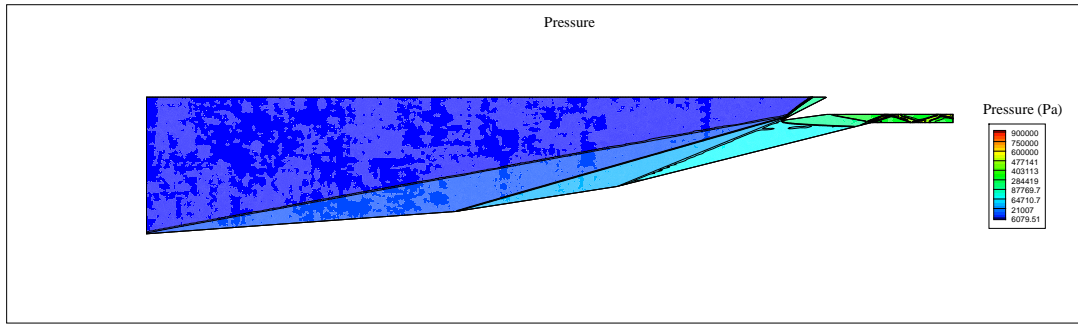
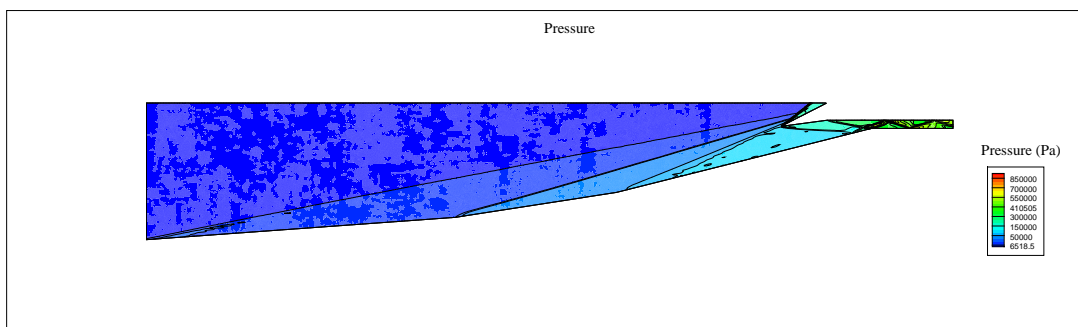Figure 3.12: Pressure contours of Mach 8 geometry (Inviscid case).

Figure 3.13: Pressure contours of Mach 8 geometry (Viscous case).

Various performance parameters of Mach 8 inlet geometry are given in Table. 3.4 for different Mach number considering 1D inviscid, 2D inviscid and viscous effects. Similar nature of results to that of Mach 6 inlet geometry is observed here. Inviscid case has over estimated the total pressure recovery as 0.829 while it is 0.53 for viscous case operated at Mach 8 and when operated at Mach 9 it is 0.56 for the viscous case. Static pressure ratio has also increased from 50.05 for 1D inviscid case at Mach 8 to 75.97 for viscous case at Mach 9.

These results suggest that when designing an inlet, 1D gas dynamic relations must not be used alone. As they are valid only for 1D cases but not when viscous effects are considered. In reality if the design is made by using these relations but not corrected for the viscous effects, there is possibility that scramjet engine might under perform and might actually fail in operation.
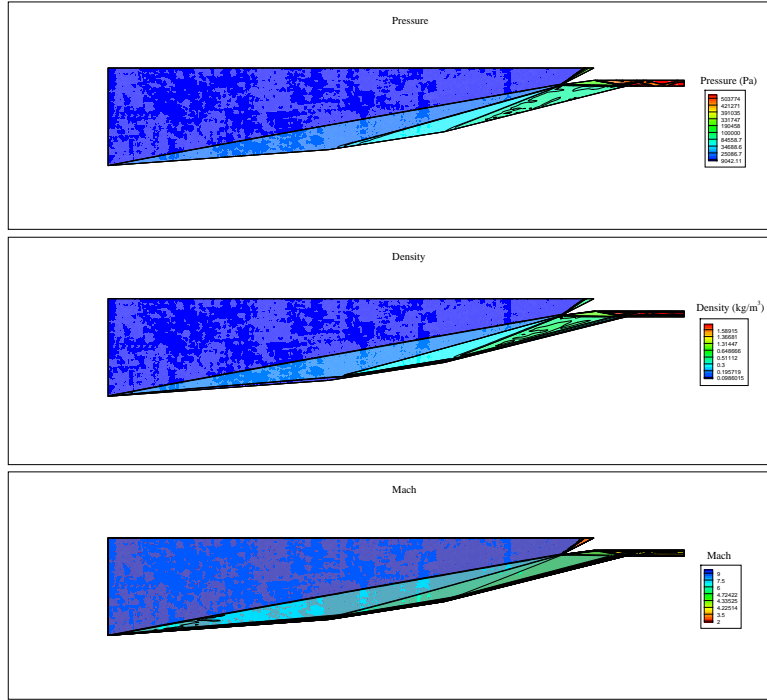
Figure 3.14: Pressure contours of Mach 8 geometry simulated at Mach 9 (Viscous case).

Table 3.4: Performance parameters of Mach 8 inlet geometry for 1D, 2D, inviscid and viscous effects

Mach	8(1D Inviscid)	8(2D Inviscid)	8(Viscous)	9(2D Inviscid)	9(Viscous)
SPR_{throat}	50.05	66.41	72.99	68.3	75.97
TPR_{throat}	0.829	0.68	0.53	0.628	0.56
M_{throat}	4	3.75	3.46	4.3	4.02
SPR_{exit}	-	64.94	79.895	65.93	87.746
TPR_{exit}	-	0.620	0.322	0.596	0.385
M_{exit}	-	3.7	3.179	4.261	3.732

3.5 Correction for viscous effects

As seen in the preceding section, when viscous effects are included the shock-on-lip condition is not satisfied at design free stream Mach number. It is found that when the inlet geometries are operated at higher Mach numbers than they are designed for, they satisfy *shock-on-lip* condition. The design Mach number is no longer what they are designed for but rather is different in viscous environment. For example, Mach 6 and Mach 8 inlets have to operate at Mach 6.5 and Mach 9 to satisfy the *shock-on-lip* condition in a viscous environment. So in order to get the correct design Mach number where in *shock-on-lip* condition is satisfied, the inviscid design algorithm specified in section. 2.2 has to be modified to include the viscous effects.

This aspect has been investigated and different inviscid inlet geometries are obtained by the current design procedure have been simulated at higher Mach number than they are designed for and the actual Mach number where in *shock-on-lip* condition is satisfied are found out. For example, Mach 7 geometry is simulated at various free stream Mach numbers in viscous environment and is found out that *shock-on-lip* is satisfied at Mach 7.8. Similarly other inlet configurations are simulated and their corresponding actual design Mach numbers are found out and it is noted that the design Mach number (M_{design}) is in linear relation with the actual design Mach number(M_{actual}) i.e. the Mach number at which *shock-on-lip* condition is satisfied. This is plotted in Fig. 3.15.
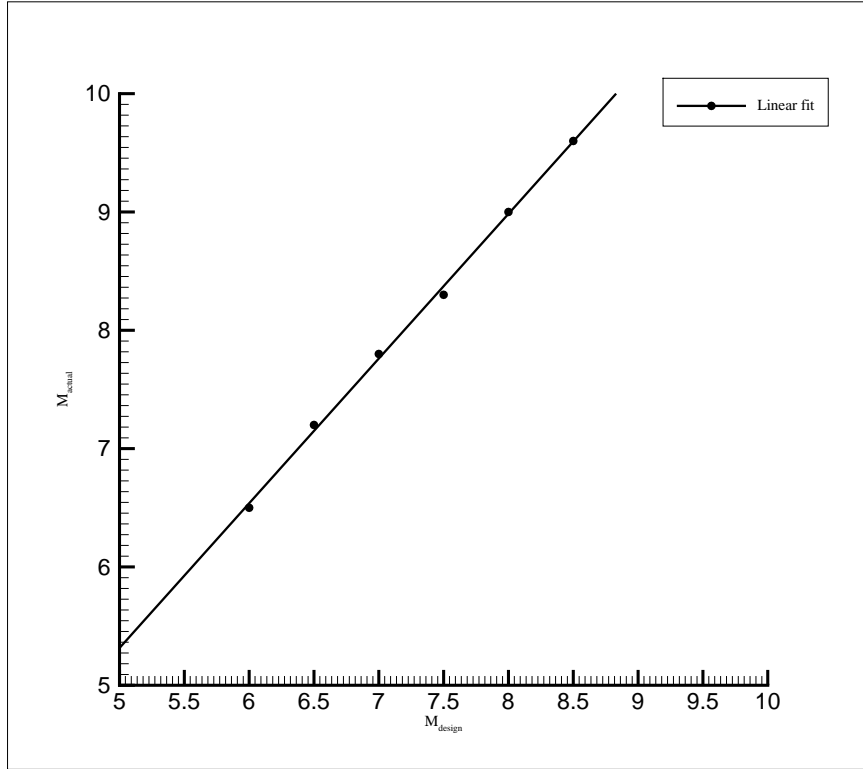

Figure 3.15: Deviation of actual Mach number from design Mach number.

From Fig. 3.15, the linear fit equation has been obtained as $M_{actual} = 1.22M_{design} - 0.799$. This correction can be included in the inviscid algorithm to obtain the actual operating free stream Mach number at which *shock-on-lip* condition is satisfied. In order to test the above relation, two scramjet inlets are designed at $M_{design} = 5, 10$ and simulated at $M_{actual} = 5.311, 11.421$ respectively as given by the above relation. The pressure contours of these results are shown in Fig. 3.16 and Fig. 3.17. As predicted, the scramjet inlets satisfy the *shock-on-lip* condition at M_{actual} given by the relation rather than at design Mach number M_{design}. By using this relation, the design methodology in section. 2.2 is corrected and scramjet inlets can be designed which can satisfy the *shock-on-lip* in a viscous
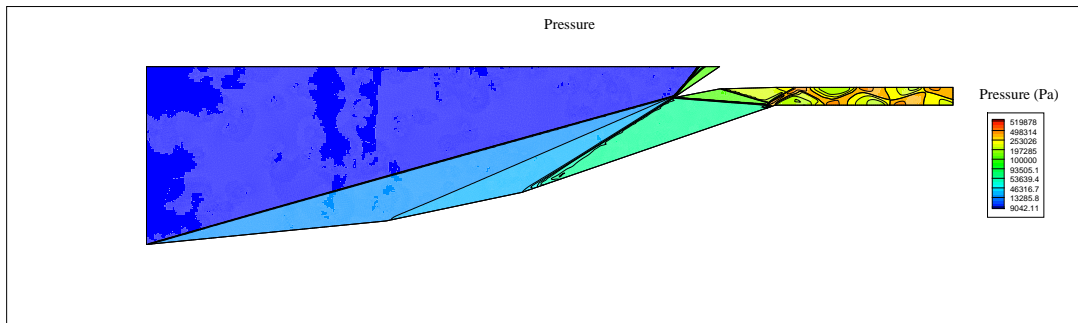
environment.

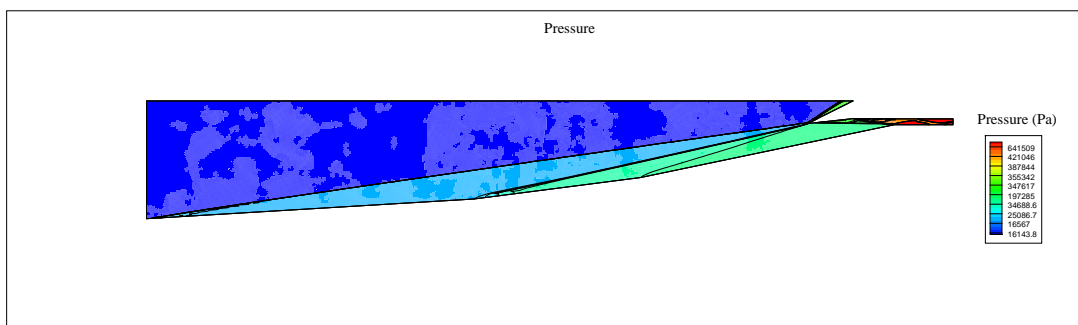Figure 3.16: Pressure contours of Mach 5 inlet operated at Mach 5.311

Figure 3.17: Pressure contours of Mach 10 inlet operated at Mach 11.421

Chapter 4

Parametric study of scramjet inlets

4.1 Effect of throat Mach number

Two scramjet inlets are designed at Mach 6 with different throat Mach numbers M_t= 40% of M_0 and M_t= 50% of M_0 and simulated at a free stream Mach number of M_0 = 6.5 for viscous case. Effects of throat Mach number on the inlet is determined. Stream line contours are plotted in Figure. 4.1. A separation region observed near the throat for the case of M_t= 40% of M_0 as reported by Mahoney[19].

Table 4.1: Performance parameters for different throat Mach numbers

M_0	6.5	6.5
M_t	$50\%M_0$	$40\%M_0$
SPR_{exit}	56.046	121.49
TPR_{exit}	0.5277	0.33
M_{exit}	2.726	2.0825

As the Mach number at the throat is decreased, strength of the external shocks increases. This is due to the fact that flow has to turn more for lesser throat Mach number than for a relatively higher Mach number at throat. This increases the backpressure at the exit of the isolator which has an effect on the inlet turning the flow backwards.

The performance parameters for different throat Mach numbers at isolator exit are given in Table. 4.1. Static pressure ratio (SPR) at the isolator exit for throat Mach of M_t=50% of M_0 is 56.04 which is two times lesser than the static pressure ratio (SPR) at isolator exit for throat Mach of M_t=40% of M_0 which is 121.49. This implies that as the throat Mach is decreases corresponding static pressure increases and leads to decrease in the overall total pressure recovery which has fallen from 0.5277 to 0.33. Hence it is much desirable to operate at higher throat Mach numbers preferably at or above M_t=50% of M_0 to avoid the separation and to improve the compression efficiency.
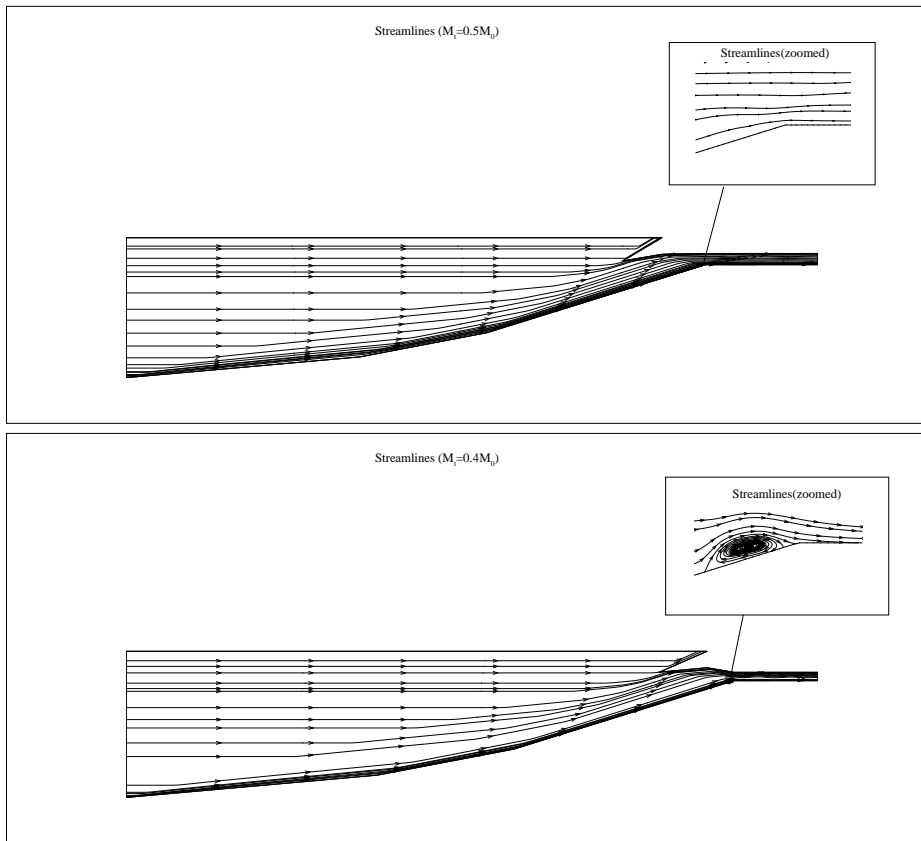
Figure 4.1: Streamline contours for Mach 6 inlet geometry operated at Mach 6.5 at different throat Mach numbers.

4.2 Effect of temperatures

Shock-shock interactions, shock-boundary layer interactions, separation are some of the phenomenon inside a scramjet inlet. This complex phenomenon might lead to decreasing in performance of a scramjet inlet. Separation can cause scramjet to unstart and control of separation regions is very important. Hence it is required to reduce these interactions between separation bubble and shock-boundary layer. One of the methods which attempt to reduce this phenomenon is wall cooling. In order to do wall cooling and to design a thermal protection system, knowledge of temperatures attained in a scramjet inlet surface is vital. To address this issue, two scramjet intake geometries are chosen and the wall temperatures are estimated and the effect of cooling on various performance parameters are studied.

Mach 10.4 inlet and Mach 7 inlet are chosen to carry out this analysis. Mach 7 inlet is obtained by the modification of geometrical parameters of Mach 6 inlet as given in Chang et.al [27]. Inlet geometry and schematic are given in section. 3.3.1 for Mach 10.4 inlet and in Fig.4.2, Table. 4.2 for Mach 7 inlet respectively. The design of Mach 7 inlet satisfies *shock-on-lip* condition. Operating conditions of Mach 10.4 are given in section. 3.3.1 and Mach 7 are as follows: free stream Mach number $M_0 = 7$, static pressure of $P_0 = 2552Pa$ and a free stream temperature of $T_0 = 215K$ is used. Unless otherwise stated, only the above operating conditions are used for the respective inlets.

Table 4.2: Geometrical parameters for Mach 7 inlet.

	x_1	x_2	x_3	x_4	x_5	x_6	L	H
Length (m)	0.212	0.113	0.083	0.0498	0.1076	0.0425	0.115	0.015
	θ_1	θ_2	θ_3	θ_4	θ_5			
Angle (deg)	6	8.3	9.9	12.4	13.8			

4.2.1 Estimation of wall temperatures

Surface temperature distribution is obtained by using adiabatic boundary condition at the surface. Surface static temperature distribution along forebody, cowl and innerbody for Mach 10.4 and Mach 7 inlets are shown in Fig. 4.3(a) and Fig. 4.3(b) respectively. The static temperature increases along the surface of the inlet due to compression process. A maximum temperature around 3280K is reached on the surface for Mach 10.4 inlet and during compression process as shown in Fig. 4.3(a) and a maximum temperature around 1850K for Mach 7 inlet as shown in Fig. 4.3(b) respectively.
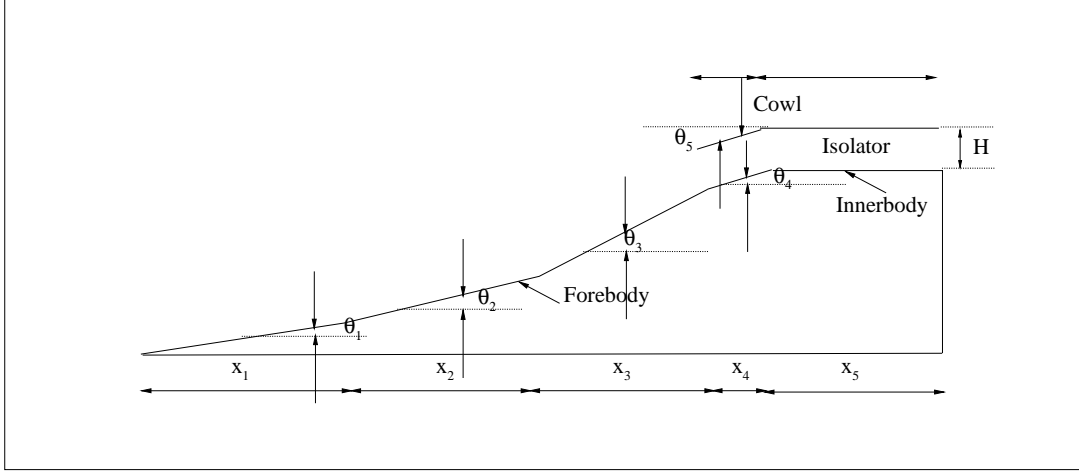
Figure 4.2: Schematic of Mach 7 inlet.

4.2.2 Effect of wall cooling

To know the effect of wall cooling on performance of scramjet inlet, simulations are performed with constant surface temperature condition. Various performance parameters of inlets at isolator exit for different wall temperatures are given in Tables. 4.3 and 4.4. Values in the tables are mass-weighted average values at the isolator exit. Total pressure recovery decreases with increase in wall temperature and the static pressure ratio is found to be increasing for both the inlets. As the wall temperature is decreased, shock and boundary layer interactions weakens and thereby increasing the total pressure recovery. The total pressure recovery has increased from 0.432 to 0.434 for Mach 10.4 inlet and 0.427 to 0.434 for Mach 10.4 and 7 inlets as the temperature is decreased from 1600K to 400K. Mach number at the isolator exit is found to be increasing from Mach 5.074 to 5.091 and Mach 3.12 to 3.189 for Mach 10.4 and 7 inlets respectively as the temperature is increased from 1600K to 400K. The decrease of temperature causes the flow uniformity at the isolator exit and also decreases the static pressure ratio. This shows that wall cooling will improve the total pressure recovery. A small change in the total pressure recovery will have a significant effect on the pressure at isolator exit.

Table 4.3: Performance parameters with different wall temperatures for Mach 10.4 inlet.

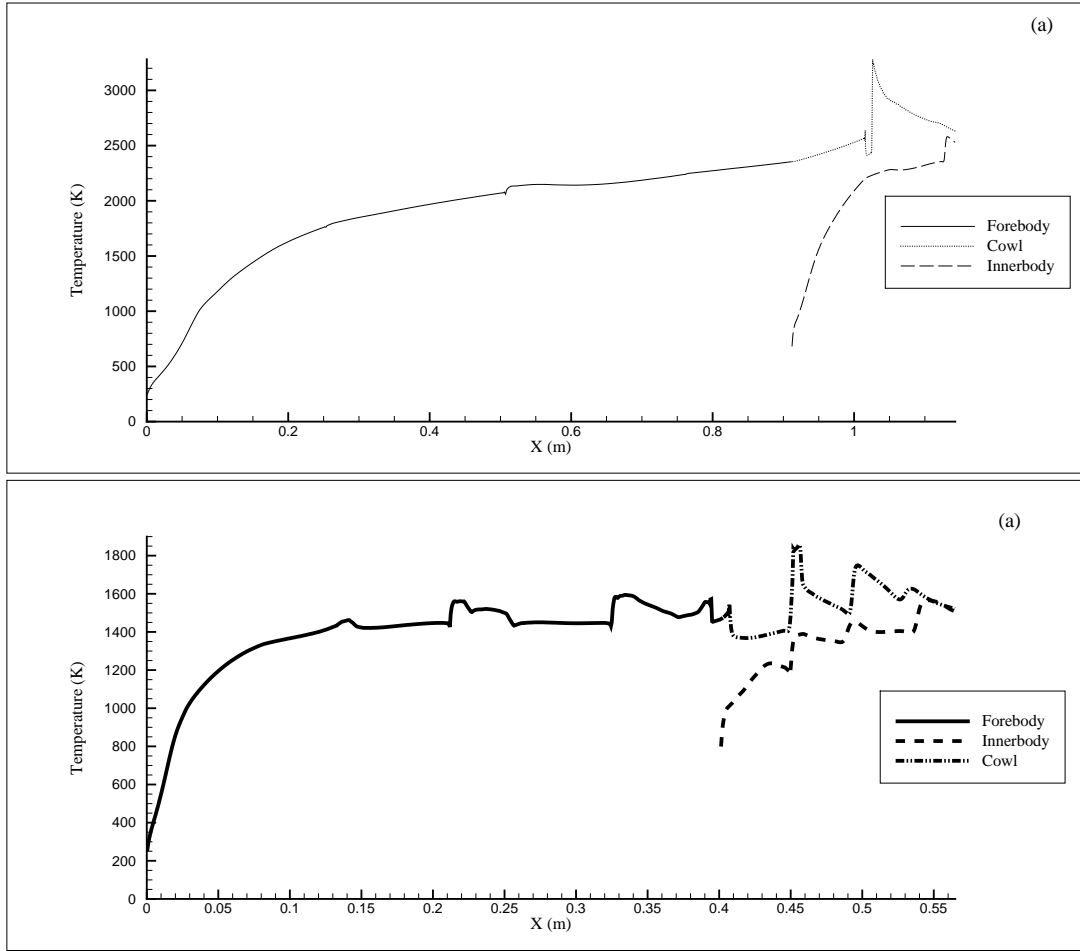| Temperature (K)	$\frac{P_{exit}}{P_0}$	$TPR = \frac{P_{t_{exit}}}{P_{t_0}}$	M_{exit}
Adiabatic	35.249	0.425	5.03
1600	34.756	0.432	5.074
1000	34.69	0.433	5.082
400	34.618	0.434	5.091

Figure 4.3: Surface static temperature distribution on (a) Mach 10.4 (b) Mach 7.

Table 4.4: Performance parameters with different wall temperatures for Mach 7 inlet.

Temperature (K)	$\frac{P_{exit}}{P_0}$	$TPR = \frac{P_{t_{exit}}}{P_{t_0}}$	M_{exit}
Adiabatic	35.69	0.423	3.088
1600	34.45	0.427	3.12
1000	33.27	0.431	3.155
400	32.01	0.434	3.189

4.3 Effect of off-design conditions

Mach 7 inlet geometry mentioned in the section. 4.2 is studied for off-design conditions. This inlet is simulated at two free stream Mach numbers Mach 6, 7. Operating conditions for Mach 7 inlet geometry are same as mentioned in the section. 4.2. Contours of Pressure for the Mach 7 inlet geometry operated at Mach 6, 7 are shown in Fig. 4.4 (a) and Fig. 4.4 (b) respectively. From Fig. 4.4 it is observed that as the inlet geometry is operated at below design condition i.e. at Mach 6, the *shock-on-lip* is no longer satisfied and the internal shock reflections inside the isolator sections becomes non-uniform when compared to the on-design condition i.e. at Mach 7 as shown in Fig. 4.4 (b). This is due to the decrease in the oblique shock angle originating from the cowl, as it moves upstream of the inlet when the inlet is operated below design condition. Also, as the Mach number is decreased below design point, the mass capture area also decreases as the spillage losses increase when the shocks become less curved.
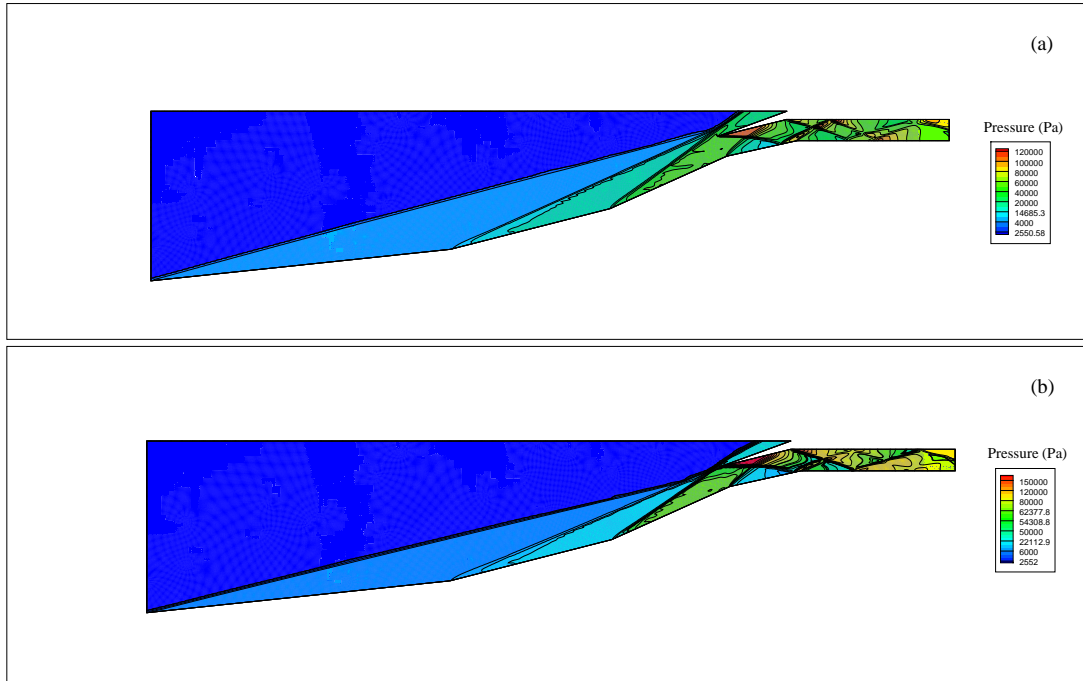

Figure 4.4: Contours of Pressure for Mach 7 inlet geometry for free stream Mach numbers (a) Mach 6 and (b) Mach 7.

Spillage loss is calculated by percentage change in the mass flow rate between inlet section and the starting section of cowl-innerbody. Spillage losses are given in Table. 4.5, where higher spillage loss imply that mass capture is poor and vice-versa. From Table. 4.5, it is observed that the spillage losses are high when the inlet is operated below design condition because as the *shock-on-lip* condition is not satisfied, less amount of air is captured

and hence the spillage loss increases. Spillage loss drops from 33.4% to 18.84% when Mach number is increased from 6 to 7. To have a better combustion efficiency, required amount of air has to be processed into the combustion chamber and in order to have a better combustion efficiency, inlet has be operated at design condition.

Table 4.5: Spillage loss with different free stream Mach numbers for Mach 7 inlet.

M_0	m_0	m_c	Spillage loss in %
6.0	9.19	6.12	33.4
7.0	10.72	8.7	18.84

Variation of total pressure recovery (TPR) at the isolator exit is for different free stream Mach numbers is shown in Fig. 4.5. It can be seen that total pressure recovery is maximum at the center due to maximum velocity of the fluid at the center. Total pressure recovery coefficient decreases with increase of Mach number due to increase of shock strengths. Various performance parameters with different free stream Mach numbers are given in Table. 4.6. TPR is 0.474 for Mach 6 and 0.431 for Mach 7 respectively. Even though the inlet is operated at design point, total pressure recovery coefficient decreases at isolator exit with increase in free stream Mach number. This is due to the fact that as the Mach number is increases, stronger shocks form and hence increase the compression ratio and there by leading to decrease in total pressure recovery.
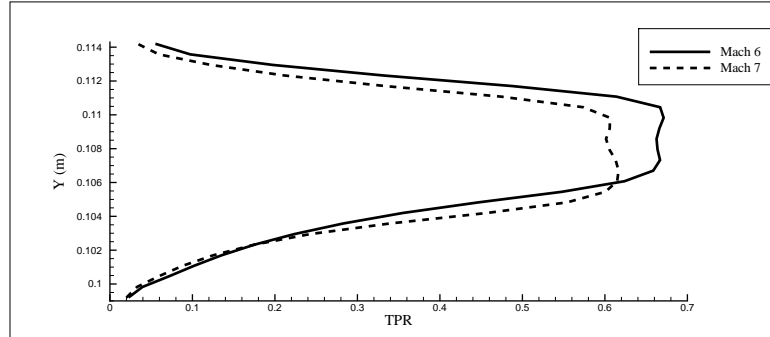

Figure 4.5: Variation of total pressure recovery coefficient (TPR) at different free stream Mach numbers for Mach 7 inlet.

Table 4.6: Performance parameters with different free stream Mach numbers for Mach 7 inlet.

M_0	$\frac{P_{exit}}{P_0}$	$TPR = \frac{P_{t_{exit}}}{P_{t_0}}$	M_{exit}
6.0	26.42	0.474	2.746
7.0	33.27	0.431	3.155

Present geometries obtained by design methodology

Scramjet inlet geometries obtained by the design methodology mentioned in section. 2.2 have been simulated for off-design conditions and spillage losses for Mach 6 and Mach 8 inlet geometries are reported in Tables. 4.7 and 4.8. For Mach 6 inlet, when the inlet is operated at Mach 6.5 i.e. at *shock-on-lip* condition, spillage losses drop from 25.10% to 17.57% and similarly for Mach 8 inlet, when the inlet operated at Mach 9 i.e. at *shock-on-lip* condition, spillage losses drop from 27.29% to 17.52%.

Table 4.7: Spillage loss with different free stream Mach numbers for Mach 6 inlet.

M_0	m_0	m_c	Spillage loss in %
6.0	44.18	33.09	25.10
6.5	47.86	39.45	17.57

Table 4.8: Spillage loss with different free stream Mach numbers for Mach 8 inlet.

M_0	m_0	m_c	Spillage loss in %
8.0	78.94	57.39	27.29
8.5	83.87	65.67	21.69
9.0	88.8	73.24	17.521

4.4 Effect of cowl height

Internal compression process starts between the cowl and the innerbody, wherein shocks originating from cowl are impinging on the innerbody which then propagate to downstream by series of shock reflections in the isolator. Cowl height is the distance measured from leading edge of the inlet to the cowl tip. Cowl height plays a major role in the compression process as it is one of the important parameters which determine the amount of compression achieved in the isolator section. For Mach 10.4 geometry, mentioned in section. 3.3.1 simulations are carried out by varying cowl height from 0.156 m to 0.144 m at operating conditions of Mach number $M_0 = 10.4$, static pressure $P_0 = 75647.65$ Pascal, free stream temperature of $T_0 = 215K$ and with a constant surface temperature of $T_w = 1000K$. The static pressure contours of current study with varying cowl heights are shown in Fig. 4.6. As the cowl height is decreased, the position where the cowl shock intersecting the innerbody moves upstream. At the minimum cowl height tested i.e. at 0.144 m, resulted in cowl shock impinging before the innerbody and causing more shock reflections inside the isolator. Surface static pressure distribution along innerbody with different cowl heights in plotted in Fig. 4.7. It is seen that as the cowl height decreases from 0.156 m to 0.144 m, static pressure on the innerbody increases due to over compression by shock reflections.
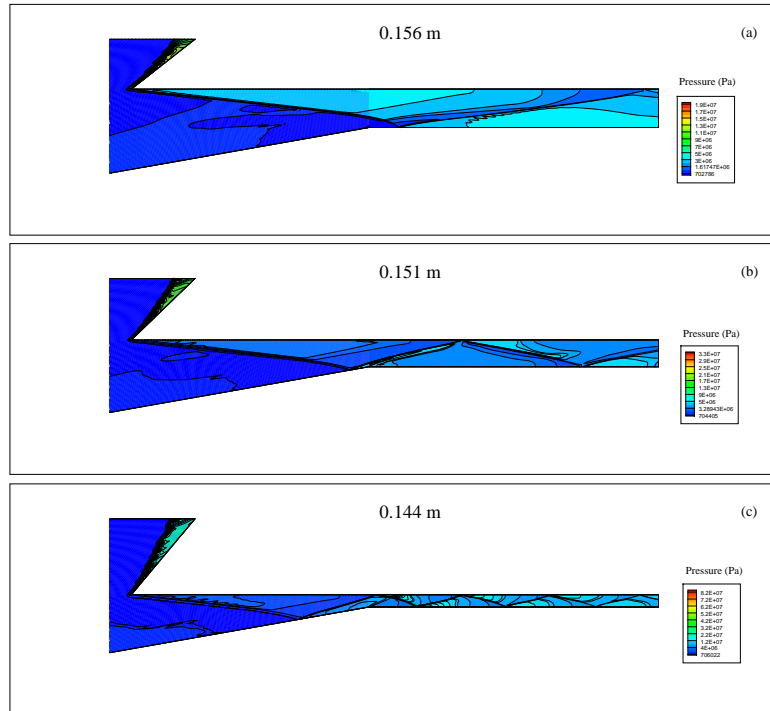

Figure 4.6: Contours of pressure at cowl heights for Mach 10.4 inlet.

Effect of the cowl height on total pressure recovery at isolator exit is shown in Fig. 4.8. As the cowl height is decreased from 0.156 m to 0.144 m, total pressure recovery coefficient
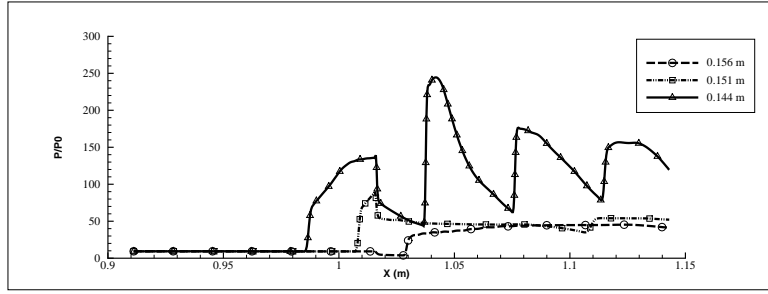
Figure 4.7: Surface static pressure distributions on innerbody with different cowl heights for Mach 10.4 inlet.

decreases due to increase in internal compression. Internal compression has increased due to increase in number of shock reflections and thereby decreasing the compression efficiency. Sudden jumps in pressures on the innerbody in Fig. 4.8 is due to the presence of shock reflections. Change in performance parameters with different cowl heights for Mach 10.4 scramjet inlet is given in Table. 4.9. TPR and Mach number decreases with decrease in cowl height due to over compression and this might lead to decrease in combustion efficiency.
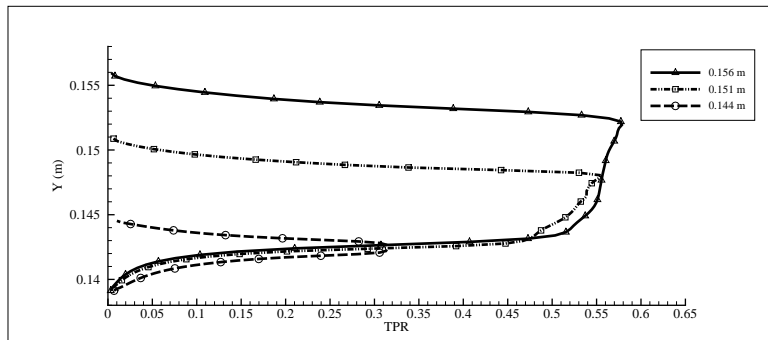

Figure 4.8: Surface static pressure distributions on innerbody with different cowl heights for Mach 10.4 inlet.

Table 4.9: Performance parameters with different cowl heights for Mach 10.4 inlet.

Cowl height (m)	$\frac{P_{exit}}{P_0}$	$TPR = \frac{P_{t_{exit}}}{P_{t_0}}$	M_{exit}
0.156	34.69	0.433	5.082
0.151	48.762	0.372	4.681
0.144	134.51	0.156	3.5

Chapter 5

External flow field analysis

A numerical study has been performed to investigate the external flow field characteristics of a scramjet vehicle. Two inlets at design Mach number 6 and 7 obtained by the design procedure in section. 2.2 and by using correction equation to find the *shock-on-lip* condition in viscous environment. The two inlets are designed satisfy the *shock-on-lip* condition in a viscous environment. In other words, Mach 6 scramjet vehicle satisfies *shock-on-lip* when operated at free stream Mach number 6 and similarly Mach 7 scramjet satisfies *shock-on-lip* at Mach 7 in a viscous environment. The inlet is extended to afterbody i.e. until the nozzle section by assuming the required lengths. A computational domain of 3 times the length of the scramjet vehicle in both x and y directions are chosen. Both the inlets are operated at their respective design Mach number 6 and 7 respectively and their operating conditions are $P_0 = 6079.5Pa$, $T_0 = 215K$.

Contours of pressure and density for Mach 6 scramjet vehicle zoomed near the scramjet vehicle is shown in Fig. 5.1 and Fig. 5.2 respectively. From the figures it is seen that external compression shocks are converging on the cowl lip and the internal compression shocks originating from the cowl are impinging on the innerbody shoulder. Isolator region is consisting of series of internal shock reflections beginning after the cowl section and extending up to the exit of combustion chamber. Here combustion chamber is considered as an extension of isolator section. Afterbody is the region after the inlet and combustor sections and is treated as nozzle. Expansion waves originate from the nozzle expansion ramps and can be seen in Figures. 5.1 and 5.2. Similarly contours of pressure and density for Mach 7 scramjet vehicle are shown in Figures. 5.3 and 5.4.
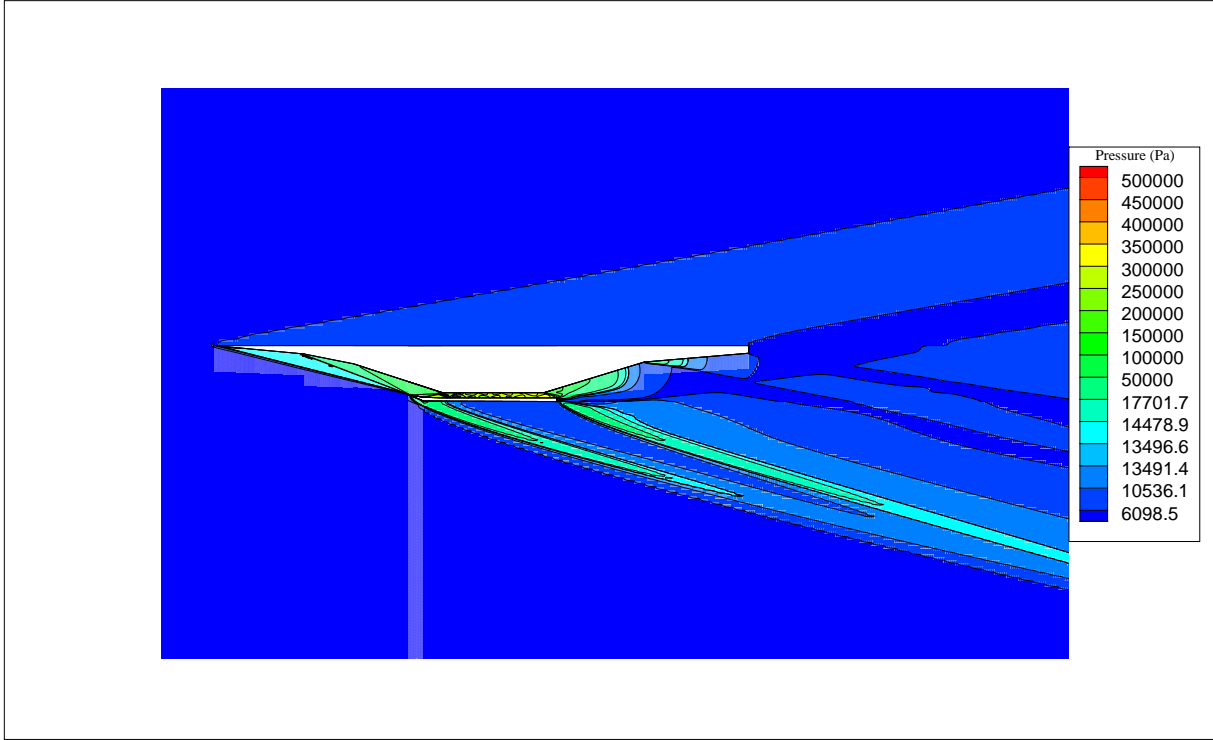
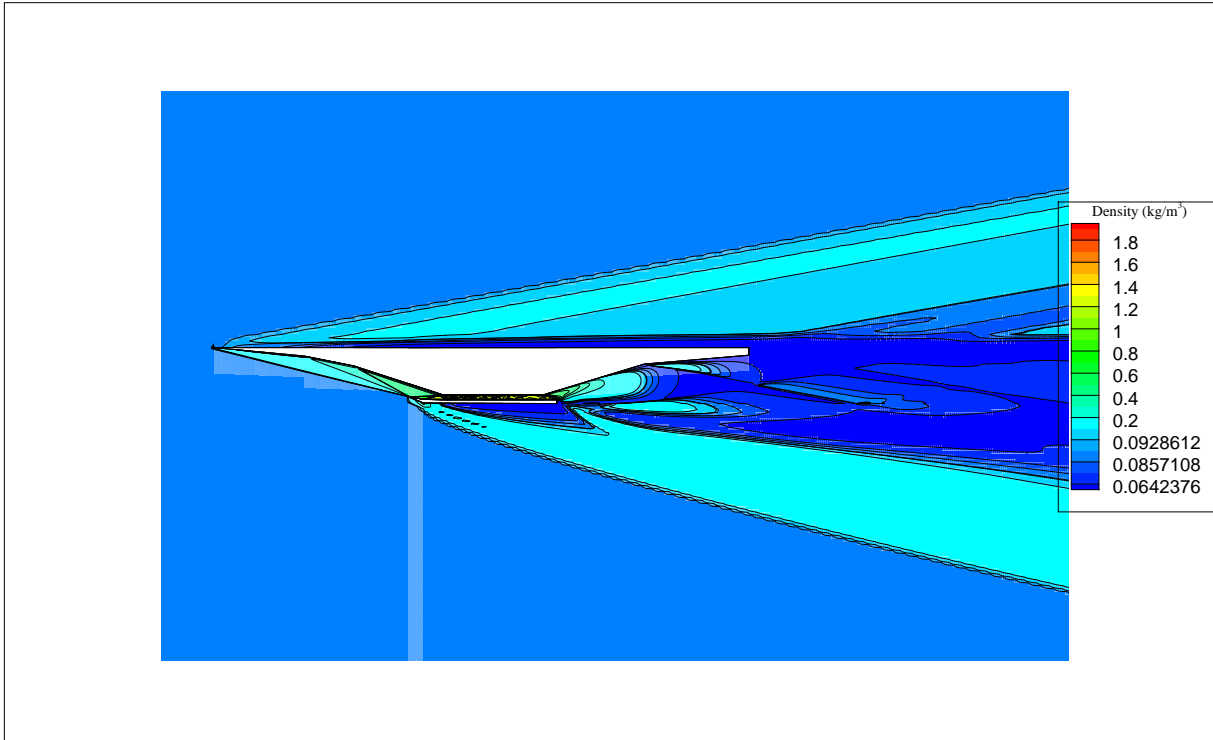Figure 5.1: Pressure contours for Mach 6 geometry.
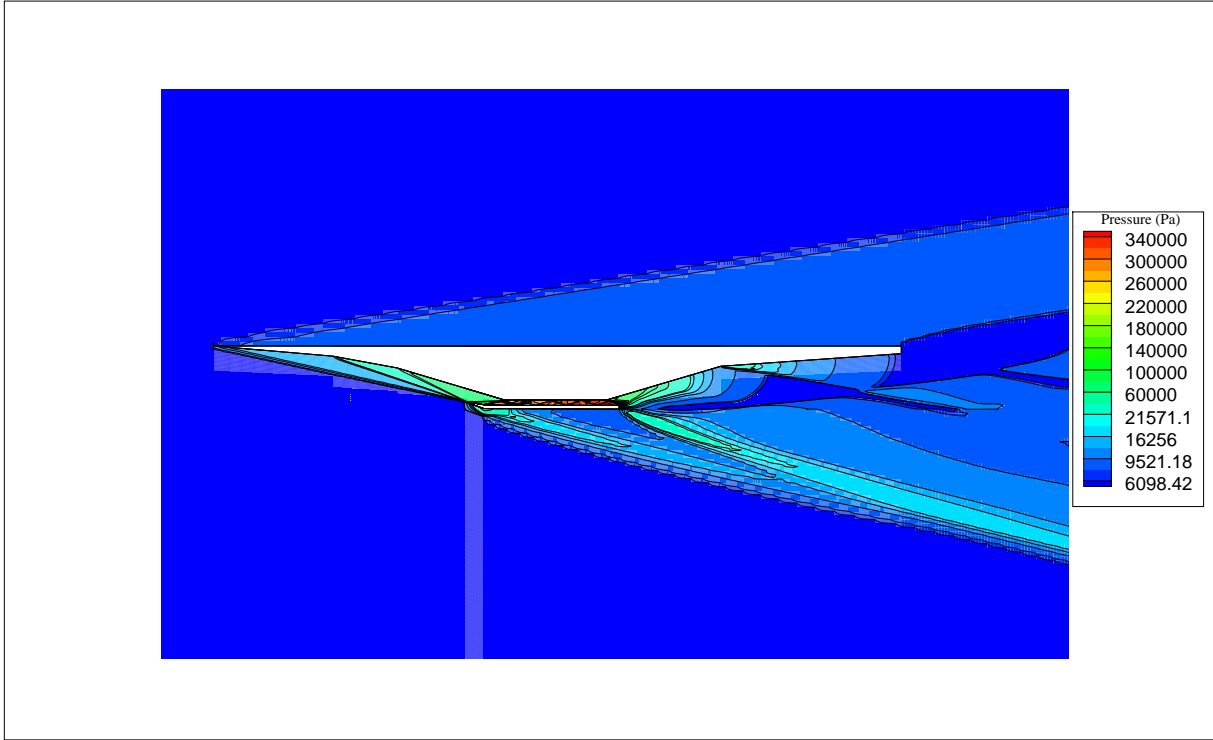

Figure 5.2: Density contours for Mach 6 geometry.

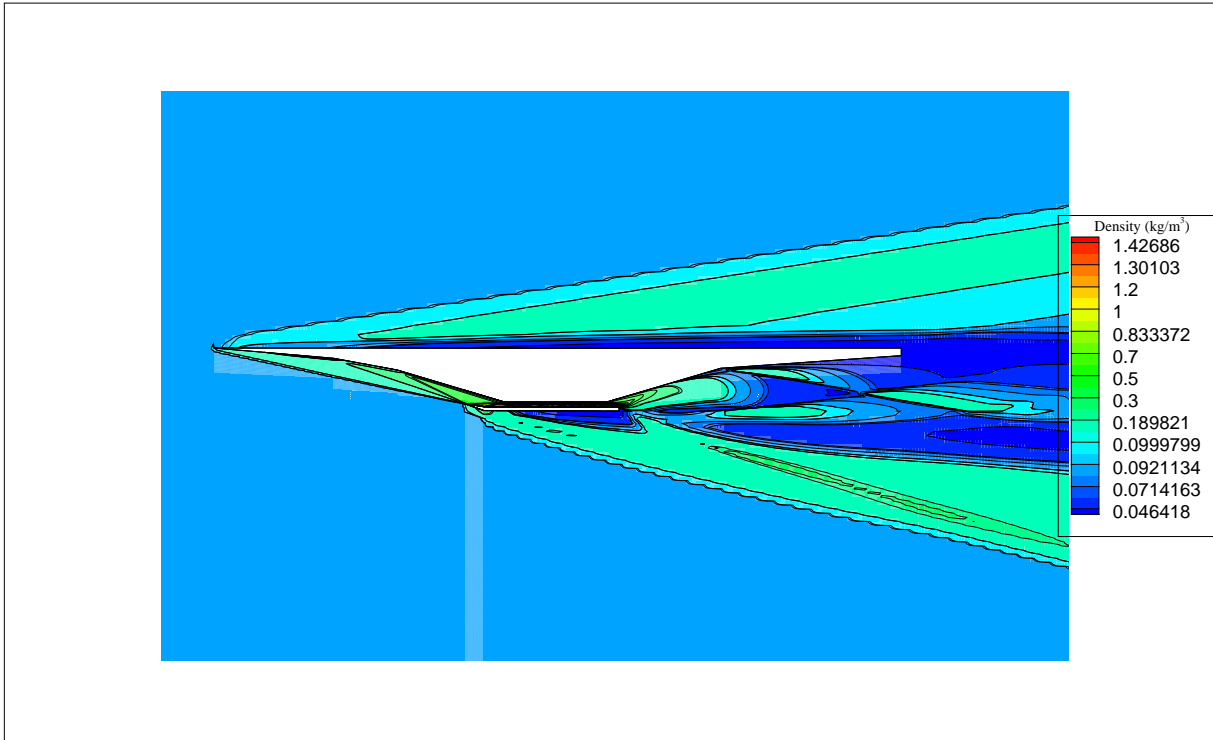Figure 5.3: Pressure contours for Mach 7 geometry.

Figure 5.4: Density contours for Mach 7 geometry.

Static pressure ratio (SPR) across the bottom part of the scramjet vehicle is plotted for Mach 6 and Mach 7 in Figures. 5.5 and 5.6 respectively. For comparison, scramjet vehicle geometries is also shown in the given figures. Due to oblique shocks, static pressure ratio increases along the inlet and into the isolator section. Sudden jumps in pressure ratio are observed between 0.9 m to 1.35 m respectively, this is the region of isolator and combustion chamber where in multiple shock reflections are present. Static pressure ratio (SPR) decreases after the combustion chamber exit i.e. at 1.35 m due to the presence of nozzle. Presence of expansion fans along the afterbody has caused the pressure ratio to decrease along the nozzle section.

Wall temperatures are estimated by Mach 6 and 7 inlet geometries as and static temperature along the bottom part of the scramjet vehicle is given in Figures. 5.7 and 5.8 for Mach 6 and 7 geometries respectively. Maximum temperatures are obtained by using adiabatic boundary condition on the wall. A maximum temperature of $1625K$ and $2080K$ is developed for Mach 6 and Mach 7 scramjet vehicles respectively. By Figures. 5.7 and 5.8 static temperature increases along the forebody and decreases along the afterbody. In these cases, effects of combustion are not included but if combustion is taken into consideration then the temperatures attained on the surface would be even higher. Especially in the afterbody region of the scramjet vehicle where thrust is produced.
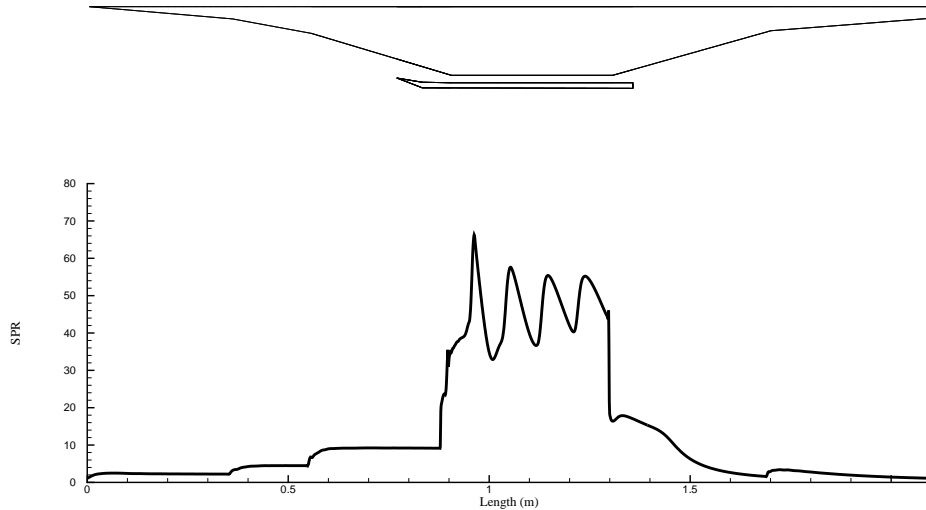

Figure 5.5: Static pressure ratio along bottom part for Mach 6 scramjet vehicle.
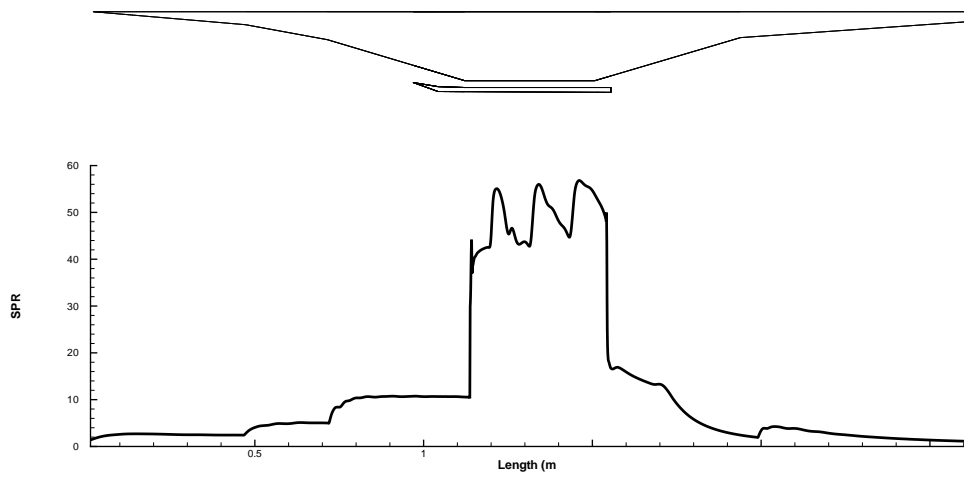
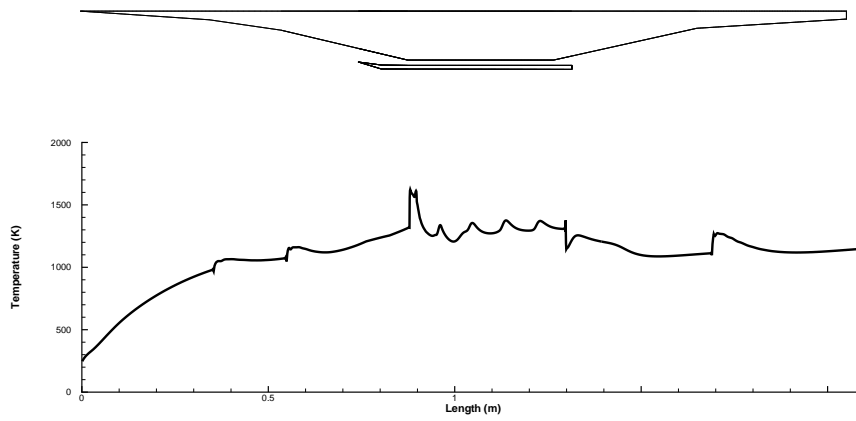Figure 5.6: Static pressure ratio along bottom part for Mach 7 scramjet vehicle.

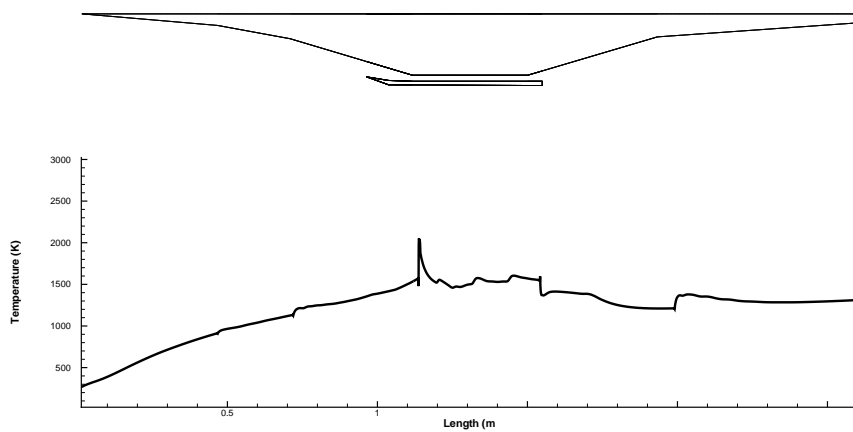Figure 5.7: Surface temperatures along bottom part for Mach 6 scramjet vehicle.

Figure 5.8: Surface temperatures along bottom part for Mach 7 scramjet vehicle.

63

Estimation of drag and lift coefficients are important to have the knowledge of the aerodynamic performance of the scramjet vehicle. Drag and lift coefficients are mainly dependent on body shape, Reynolds number and Mach number. Hence the shape of scramjet is vital in determining the aerodynamic performance of the scramjet vehicle. Coefficient of drag and lift for present Mach 6 and Mach 7 scramjet vehicles is given in Table. 5.1. It is known that as velocity increases, drag drag coefficient decreases and similar nature is observed here. Coefficient of drag for Mach 6 scramjet is 0.158 but for Mach 7 scramjet it is 0.1375. As the Mach is increased, coefficient of drag and lift have decreased where as the ratio of coefficients of lift to drag has increased. Drag and lift coefficients are given for a Mach 7 inlet at an angle of attack 2 degrees by Sun et.al [33] as 0.26 and 0.3 respectively. Present drag and lift coefficients are comparatively less than the ones obtained by Sun et.al [33]. The present geometry and the geometry of Sun et.al [33] are different and a direct comparison cannot be made, but a knowledge of lift and drag coefficients are obtained.

Table 5.1: Drag and lift coefficients for Mach 6 and 7 scramjet vehicles.

Mach	c_d	c_l	$\frac{c_l}{c_d}$
6	0.158	0.3145	1.99
7	0.1375	0.2872	2.08

Chapter 6

Conclusions

A new methodology has been developed for the design of hypersonic scramjet inlet and is reported in the present study. In the literature design of scramjet inlet has been done by either maximize the total pressure recovery or prescribing Mach number at the throat. Present investigation has combined the above two approaches and obtained the optimal inlet geometry which has maximum total pressure recovery at a prescribed free stream Mach number. Designed scramjet inlet geometries are simulated and performance parameters are reported for various parameters such as 1D, 2D, invsicid and viscous effects. Present simulations are able to capture the flow field characteristics such as oblique shocks, shock/boundary layer interactions and shock reflections.

Total pressure recovery which determines the inlet efficiency is higher in the present approach than the previous approaches. Turning angles decrease with an increase of external/internal shocks due to decrease of shock strength. The efficiency of the inlet increases with an increase of external/internal shocks. There is a significant deviation in performance parameters of inlet in 1D, 2D, inviscid and viscous analysis. Present results show that 2D and viscous effects have to be considered for design of scramjet inlets. The *shock-on-lip* condition which is imposed by the design methodology but this does not satisfy in the viscous flow field due to shock-shock and shock/boundary layer interactions. A correction equation is given which finds the actual Mach number that satisfies the *shock-on-lip* condition. Present results agree with the experimental results of Wan Vie and Ault[25]. As predicted by Mahoney[19] it has also been shown that separation region is formed if Mach number at the throat is decreased below 50% of M_0.

Performance parameters of scramjet inlet are reported for various parameters such as cowl height, wall temperature and free stream Mach number. The performance of inlet can be improved by wall cooling due to weakening of shock-wave/boundary layer interactions. Total pressure recovery coefficient and Mach number at isolator exit decreases with decrease in cowl height due to increase of internal shock reflections and hence cowl height is one of

the important performance parameter. Spillage loss is high when the inlet is operated below design Mach number due to shock-on-lip condition not being satisfied and hence required amount of air will not enter into the combustion chamber. Pressure and temperature distributions along the surface for two different scramjet vehicles have been reported. Drag and lift coefficients have been obtained for Mach 6 and Mach 7 scramjet vehicles. The results in the current study are useful in designing hypersonic scramjet inlets and in understanding the flow behavior of scramjet inlets.

Chapter 7

Future work

An interesting continuation for the present study would be to extend the scramjet inlet to include the combustion chamber and the nozzle afterbody and study various flow field phenomenons. The effects of backpressures from the combustion chamber on the compression efficiency of the scramjet inlet can be studied and a restriction can be imposed on the length of the isolator which can prevent / contain the adverse pressure gradients from propagating into the scramjet inlet. Another aspect is to study the inlet unstart phenomenon and its dependencies on various parameters such as contraction ratio, separation bubbles, backpressures and various flow field characteristics such as shock/boundary layer interactions. Dependency of aerodynamic performance parameters such as lift and drag coefficients of the scramjet vehicle on the inlet start and unstart conditions can also be studied. High temperature / real gas effects, chemically reacting flows and low density effects can be considered to accurately estimate various flow field parameters of the scramjet vehicle.

Another interesting aspect would be to study various cooling techniques for a scramjet vehicle. As very high temperatures are developed on the surface of a scramjet vehicle, there is a great need to develop a thermal protection system so as to protect the scramjet vehicle. In this aspect, study of various configurations of cooling channels attached to the scramjet vehicle and thermodynamic study of cooling cycles that can be employed can be done.

Supersonic combustion being the key characteristic of a scramjet engine and the analysis of flow field inside the combustion chamber in presence of chemically reacting fluid can be carried out. Various fuel injection methods and injector configurations can also be studied and an optimum injector configuration which does the proper mixing of the fuel and the fluid can be obtained. By this an accurate estimation of temperatures developed inside a combustion chamber can be made and this information can be used to develop thermal protection systems. Also the information of the exhaust gases and their velocities is very much important in evaluating the thrust and efficiency of the combustion. As the combustion efficiency is also related to the compression efficiency, inlet geometry can be adjusted to

add the effects of combustion and improve the overall compression-combustion efficiency.

Similar to the design of inlet geometry which improves the compression efficiency (which is carried out in this study), scramjet nozzle can be designed to improve the overall thrust efficiency of the scramjet vehicle. The geometrical contour of the scramjet nozzle determines the properties of expansion waves that are produced along the nozzle and hence affects the conditions after the combustion chamber. When the geometrical contour of the nozzle is optimized, indirectly thrust produced will also improve and thereby improving the vehicle performance. Various configurations such as Single Expansion Ramp Nozzle (SERN), Double Expansion Ramp Nozzle (DERN) can be considered and their effects on nozzle performance can be studied.

Finally, complete scramjet vehicle integration can be done by combining inlet, combustion chamber and nozzle sections and the overall scramjet vehicle flow field analysis can be carried out with optimized inlet and nozzle and with combustion activated. This attempts to optimize the whole scramjet as an entity and yields in more accurate prediction of complete flow field around and inside a scramjet vehicle and helps in better design and operation of a scramjet vehicle.

References

[1] Robert D.Zucker, Oscar Biblarz "Fundamentals of gas dynamics" John Wiley and Sons, (2002).

[2] M.K.Smart, Scramjets. In Advances on Propulsion Technology for High-Speed Aircraft *Educational Notes* RTO-EN-AVT-150, (2008), pp. 9-1 9-38.

[3] Andrews, E. H., Mackley NASAs Hypersonic Research Engine Project A review *NASA*, TM-107759, (1994).

[4] Gordon L. Dugger, Frederick S. Billig "Supersonic ramjet missile" US PATENT 4291533, (1981).

[5] M.K.Smart, "Scramjet Inlets" RTO-EN-AVT-185

[6] E.T. Curran, S.N.B. Murthy, Scramjet Propulsion, Progress in Astronautics and Aeronautics, 189, AIAA ,2000.

[7] W.H. Heiser, D.T. Pratt, Hypersonic air breathing propulsion, AIAA, (1993) 251-257.

[8] Mauro Valorani, Francesco Nasuti, Marcello Onofri, Carlo Buongiorno, Optimal Supersonic intake design for air collection engines, *Acta Astronautica*, 45(12), (1999) 729-745 .

[9] K. Oswatitsch Pressure Recovery for Missiles with Reaction Propulsion at High Supersonic Speeds (the Efficiency of Shock Diffusers), *NACA*, TM 1140 (translation), (1947).

[10] M.K. Smart, Optimization of two dimensional scramjet inlets, *Journal of Aircraft*, 36(2), (1999) 430-433.

[11] F.S. Billig, Research on supersonic combustion, *Journal of Propulsion and Power*, 9(4), (1993) 499-514.

[12] F.S. Billig, A.P. Kothari, Stream line Tracing: Technique for designing hypersonic vehicles, *Journal of Propulsion and Power*, 16(3), (2000) 465-471.

[13] B.U. Reinartz, C.D. Hermann, Aerodynamic performance analysis of a hypersonic inlet isolator using computation and experiment, *Journal of Propulsion and Power*, 19(5), (2003) 868-875.

[14] Ge-Chang Zha, Donald Smith, Mark Schwabacher, Khaled Rasheed, Andrew Gelsey, Doyle Knight, High performance missile inlet design using automated optimization, *Journal of Aircraft*, 34(6), (1997) 697-705.

[15] XuXu, XuDajun, CaiGuobio, Optimization design for scramjet and anlaysis of its operation performance, *Acta Astronautica*, 57, (2005) 390-403.

[16] A. Kantrowitz, C.Donaldson, Preliminary Investigation of Supersonic Diffusers, *NACA*, WRL-713 (1948).

[17] M.K. Smart, C.A. Trexler, Mach 4 Performance of a Fixed-Geometry Hypersonic Inlet with Rectangular-to-Elliptical Shape Transition, *Journal of Propulsion and Power*, 20(2), (2004) 288-293.

[18] J.M. Delery, Shock wave/Turbulent boundary layer interaction and its control, *Progress in Aerospace Sciences*, 22, (1985) 209-280

[19] J.J. Mahoney, Inlets for supersonic missiles, *AIAA Education series*, Washington DC, (1993).

[20] E.H. Andrews, C.R. Mc Clinton, S.Z. Pinckney, Flowfield Starting Characteristics of an Axisymmetric Mixed Compression Inlet, NASA TH-X-2072, 1971.

[21] D.M. Van Wie, F.T. Kwok, R.F. Walsh, Starting characteristics of supersonic inlets, AIAA-2914,1996.

[22] Juntao Chang, Daren Yu, Wen Bao, Yi Fan, Operation pattern classification of hypersonic inlets, *Acta Astronautica*, 65, (2009) 457-466.

[23] A. Hamed, J.S. Shang, Survey of validation database for shockwave boundary layer interactions in supersonic inlets, *Journal of Propulsion and Power*, 7(4), (1991) 617-624.

[24] J.L. Stollery, Some aspects of shock-wave/boundary layer interaction relevant to intake flows, Hypersonic combined cycle propulsion, AGARD-CD-479, (1990).

[25] D.M. Van Wie, D.A. Ault, Internal flow field characteristics of a scramjet inlet at Mach 10, *Journal of Propulsion and Power*, 12(1), (1996) 158-164.

[26] E. Daniau, M. Sicard, Experimental and numerical investigations of an endothermic fuel cooling capacity for scramjet application, AIAA-3404,(2005).

[27] Juntao Chang, Wen Bao, Daren Yu, Yi Fan, Yi shen, Effects of wall cooling on performance parameters of hypersonic inlets, *Acta Astronautica*, 65, (2009) 467-476.

[28] M.K. Smart, Design of Three-Dimensional Hypersonic Inlets with Rectangular-to-Elliptical Shape Transition, *Journal of Propulsion and Power*, 15(3), (1999) 408-416 .

[29] M.K. Smart, Experimental Testing of a Hypersonic Inlet with Rectangular-to-Elliptical Shape Transition, *Journal of Propulsion and Power*, 17(2), (2001) 276-283 .

[30] J. Haberle, A. Gulhan, Investigation of two-dimensional scramjet inlet flow field at Mach 7, *Journal of Propulsion and Power*, 24(3), (2008) 446-459.

[31] L.A. Povinelli, Advanced computational techniques for hypersonic propulsion, *NASA*, TM-102005, (1989).

[32] M E White, J P Drummond, A Kumar Evolution and application of CFD techniques for scramjet engine analysis, *Journal of Propulsion and Power*, 3(5), (1987) 423-439.

[33] Sun Shu, Zhang Hongying, Cheng Keming, Wu Yizhao The Full Flowpath Analysis of a Hypersonic Vehicle, *Chinese Journal of Aeronautics*, 20, (2007) 385-393.

[34] Charles E Cockrell, Lawrence D Huebner Generic hypersonic inlet module analysis *AIAA*, 91-3209, (1991).

[35] D R Reddy, G E Smith, M F Liou, Thomas J Benson Three dimensional viscous analysis of a hypersonic inlet, *NASA*, TM-101474, (1989).

[36] Scott D Holland, Mach 10 computational study of a three-dimensional scramjet inlet flow field *NASA*, TM-4602, (1995).